iScience

Article

Elevated zygotic let-7f-5p alters developmental trajectories and sex-specific somatic growth

Graphical abstract

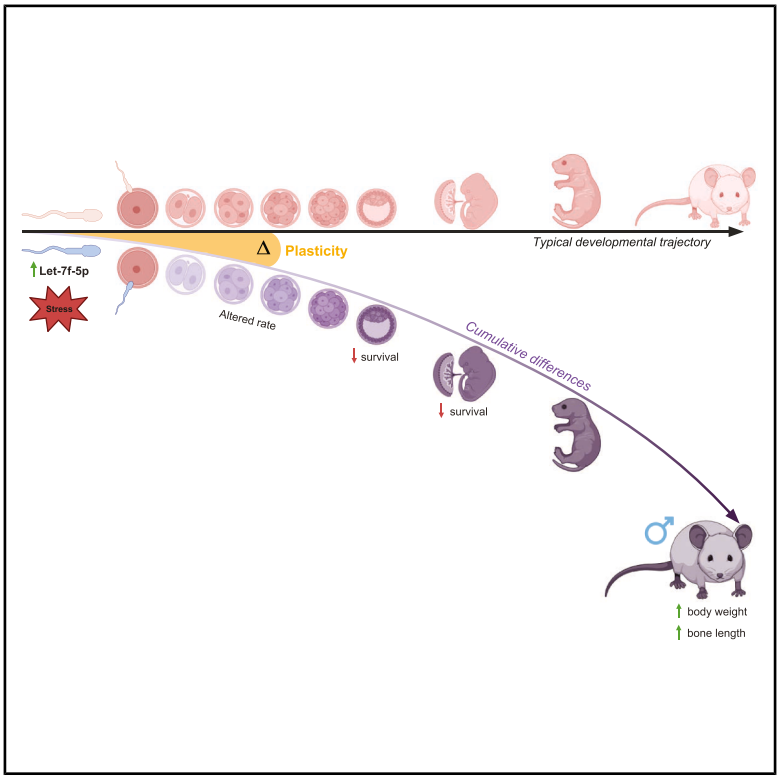

Highlights

- Elevated let-7f altered developmental rates, reducing embryonic and fetal survival
- Early transcriptomic changes were enriched for metabolic and growth pathways
- Male let-7f adult offspring had significantly greater body weight and tibia length

Authors

Alyssa C. Jeng, Kerstin C. Creutzberg, Arthur S. Feltrin, Nickole Moon, Nicolae A. Leu, C. Neill Epperson, Tracy L. Bale

Correspondence

tracy.bale@cuanschutz.edu

In brief

Molecular biology; Developmental biology

Jeng et al., 2026, iScience *29*, 116115
June 19, 2026
https://doi.org/10.1016/j.isci.2026.116115

CellPress

iScience

CellPress
OPEN ACCESS

Article

Elevated zygotic let-7f-5p alters developmental trajectories and sex-specific somatic growth

Alyssa C. Jeng,[1] Kerstin C. Creutzberg,[1] Arthur S. Feltrin,[1] Nickole Moon,[1] Nicolae A. Leu,[1] C. Neill Epperson,[1] and Tracy L. Bale[1,2,*]

[1]Department of Psychiatry, University of Colorado Anschutz Medical Campus, Aurora, CO 80045, USA
[2]Lead contact
*Correspondence: tracy.bale@cuanschutz.edu
https://doi.org/10.1016/j.isci.2026.116115

SUMMARY

Parental preconception experiences shape offspring development and longitudinal health outcomes, including disease risk. In a longitudinal human cohort, we previously identified sperm let-7f-5p (let-7f) as significantly increased in response to elevated prior perceived stress. As microRNAs (miRNAs) are causal agents in the germline transmission of prior paternal experience, we investigated developmental outcomes altered by increased let-7f using mouse zygote microinjection. Let-7f embryos developed at a faster rate until stalling at the morula stage, resulting in reduced blastocyst survival. Blastocyst and fetal RNA sequencing revealed significant differences in gene expression enriched for metabolic and growth pathways, effects that were limited to male offspring. Sex-specific developmental differences persisted into adulthood, with significantly increased body weight and bone length in let-7f males. These results demonstrate that increased let-7f shapes embryo development and male fetal and adult growth, advancing our understanding of how parental experiences may facilitate offspring developmental plasticity.

INTRODUCTION

Evidence from human epidemiological studies indicates that parental exposures shape offspring development and contribute to longitudinal health outcomes.[1–15] More recently, focus on the influence of paternal experiences on offspring health has grown. Notably, in recent human and rodent model studies, paternal preconception experiences, including altered diet, exercise, drug and toxin exposure, age, stress, and infection, were linked to differences in offspring cardiovascular health, metabolic function, behavioral measures, neurodevelopment, and mental health outcomes.[4–8,11,13,14,16–31]

Recent mechanistic studies have focused on small noncoding RNAs (sncRNAs), including microRNAs (miRNAs), as causal agents in the transmission of paternal exposures at conception.[32–35] miRNA, specifically, play an important role in sperm maturation, fertilization, and preimplantation embryo development.[32,36–39] Additionally, miRNAs regulate hundreds of mRNA targets, allowing for simultaneous and widespread coordination of gene expression post-fertilization. Our laboratory and others previously reported that sperm miRNAs were responsive to environmental perturbations, uniquely positioning them as communicators of paternal experiences thereby functioning as regulators of offspring development.[28,29,31,40–42]

In a healthy subject repeated measures longitudinal study, we previously identified let-7f-5p (let-7f) as a key sperm miRNA that was normally lowly expressed across men but was elevated in response to increased prior perceived stress.[40] Let-7 isoforms are highly conserved across species and play important roles in cell differentiation and development.[43–50] Thus, let-7f may serve as an evolutionarily conserved response signal able to shape the trajectory of embryo and fetal development to reflect paternal experience. Such plasticity in early development would provide a mechanism for an organism to be well suited to their expected environment.[51–54] However, how and when elevated let-7f modifies development or results in lasting offspring outcomes remains unclear.

Therefore, to examine the developmental impact of let-7f post-fertilization, we microinjected let-7f into mouse zygotes and examined blastocyst transcriptomics and developmental outcomes using time-lapse imaging. Embryo and fetal sex were assessed as a key variable in effects of elevated let-7f. Finally, adult offspring were examined for phenotypic differences focused on predictions from developmental findings.

RESULTS

Let-7f zygotic microinjection alters embryo survival and the blastocyst transcriptome

To determine how elevated let-7f impacts early embryo development, we microinjected mouse zygotes with a vehicle or a let-7f mimic. We utilized 2 concentrations of let-7f, a concentration based on stressed men (let-7f) and twice that (2× let-7f) to validate the specificity of our mimic (Figure 1A). As the blastocyst represents the earliest stage where distinct cell lineages emerge (i.e., trophectoderm [TE] and inner cell mass [ICM]), we first examined this stage (Figure 1A). Overall, we detected a significant reduction in the percent of embryos that reached the

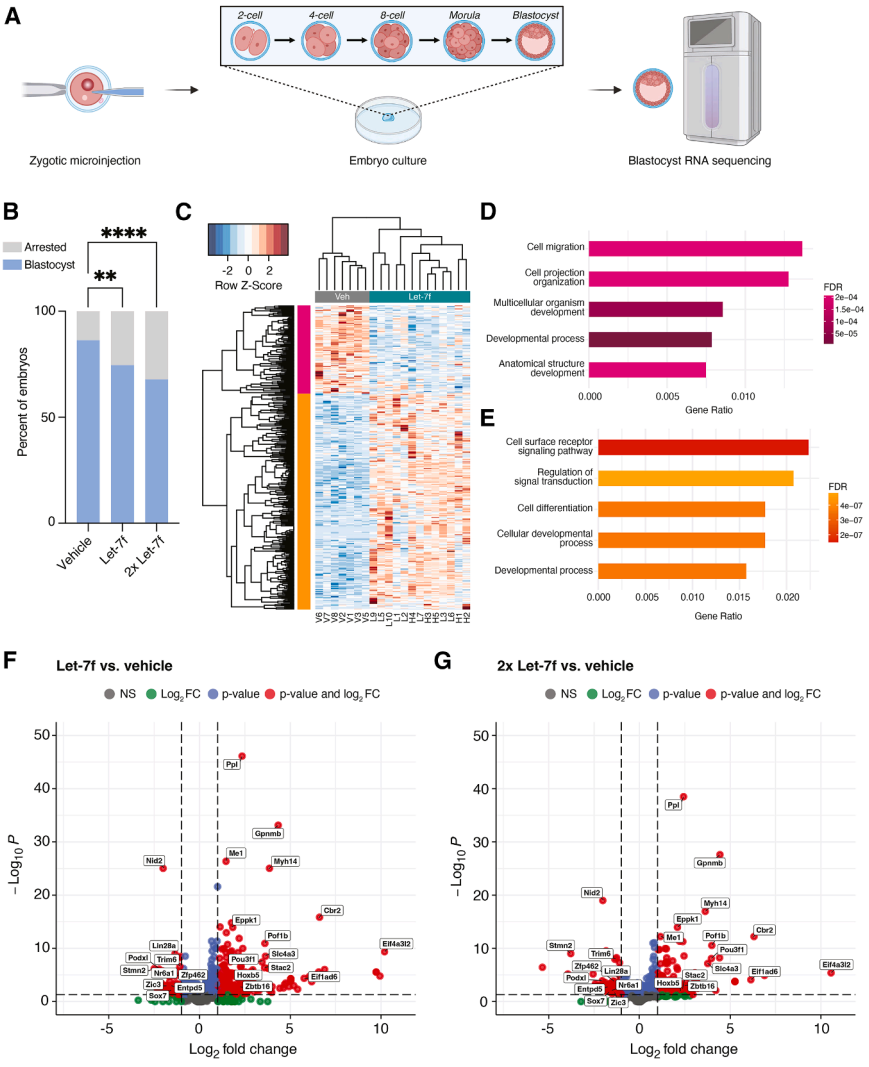

Figure 1. Increased levels of let-7f at the zygote stage impaired embryo development and altered the blastocyst transcriptome

(A) Schematic representation of the microinjection paradigm. Zygotes were randomly assigned to microinjection of vehicle, let-7f, or 2× let-7f. Embryos were cultured until the blastocyst stage, and N = 10 blastocysts were pooled per biological replicate prior to RNA isolation and sequencing.

(B) Percent of injected embryos that arrested or reached the blastocyst stage (vehicle N = 182, let-7f N = 220, 2× let-7f N = 171; chi-square test, $^{**}p$ = 0.0035, $^{****}p < 0.0001$).

(C) Heatmap of 383 DEGs between vehicle (N = 7 pooled) and let-7f groups (let-7f N = 8 pooled, 2× let-7f N = 5 pooled). Unbiased hierarchical clustering of samples and genes are visualized by dendrogram. Pink cluster contains genes downregulated in let-7f groups, and orange cluster contains genes upregulated in let-7f groups. Vehicle samples are denoted by "V," let-7f samples are denoted by "L," and 2× let-7f samples are denoted by "H".

(D and E) Plots visualizing overrepresented biological processes in (D) pink cluster and (E) orange cluster as determined by GO functional enrichment analysis.

(F and G) Volcano plots showing DEGs between (F) let-7f and vehicle and (G) 2× let-7f and vehicle. For all, DEGs have $\log_2$ fold change $\geq |1|$ and adjusted $p \leq 0.05$.

(A) created with BioRender.com released under a Creative Commons Attribution-NonCommercial-NoDerivs 4.0 International license (https://creativecommons.org/licenses/by-nc-nd/4.0/deed.en).

blastocyst stage in both let-7f groups ($X^2(2) = 17.12$, $p = 0.0002$) (Figure 1B). Post hoc analyses revealed significant differences between vehicle and let-7f embryos ($X^2(1) = 8.501$, $p = 0.0035$) and vehicle and 2× let-7f embryos ($X^2(1) = 17.08$, $p < 0.0001$) but no differences between let-7f and 2× let-7f embryos ($X^2(1) = 2.130$, $p = 0.1444$) (Figure 1B).

As miRNAs primarily function to regulate gene expression, we analyzed the blastocyst transcriptome to look for changes propagated by elevated let-7f using RNA sequencing. 10 embryos were pooled per biological replicate to provide adequate material for high-quality RNA isolation. In comparing both let-7f groups to the vehicle, we found 383 differentially expressed genes (DEGs) (Figure 1C). Hierarchical clustering demonstrated that both concentrations of let-7f impacted gene expression in similar ways, supporting the specificity of this mimic (Figure 1C). The pink cluster included 109 downregulated genes, and the orange cluster included 267 upregulated genes (Figure 1C; Table S1). We compared the downregulated DEGs with predicted let-7f targets and found an overlap of 12 genes, indicating canonical action of our mimic (Figure S1A). To gain biological insight into the blastocyst DEGs, we performed Gene Ontology (GO) functional enrichment analysis. This approach allowed us to identify biological processes that were statistically overrepresented in each cluster, highlighting functional themes that may underlie the observed transcriptional changes. Within both clusters, we saw significant enrichment for processes related to early development, such as cell migration, anatomical structure development, and cell differentiation (Figures 1D and 1E; Table S1).

In comparing the let-7f treatment groups to the vehicle separately, differential gene expression analysis revealed 204 upregulated and 68 downregulated DEGs between let-7f and vehicle (Figure 1F). Similarly, 187 upregulated and 72 downregulated genes were differentially expressed between 2× let-7f and vehicle (Figure 1G). Between these two pairwise comparisons, we found 148 shared DEGs, including 117 upregulated and 31 downregulated genes (Figure S1B). Hierarchical clustering among these shared DEGs again demonstrated similar effects of both let-7f concentrations on blastocyst gene expression (Figure S1C). Within the cluster of downregulated genes, we observed important developmental genes, including *Lin28a*, *Nr6a1*, *Sox7*, and *Trim6*, and genes for several zinc-finger proteins, such as *Zic3* and *Zfp462* (Figures 1F and 1G; Table S1). Within the cluster of upregulated genes, we noted various

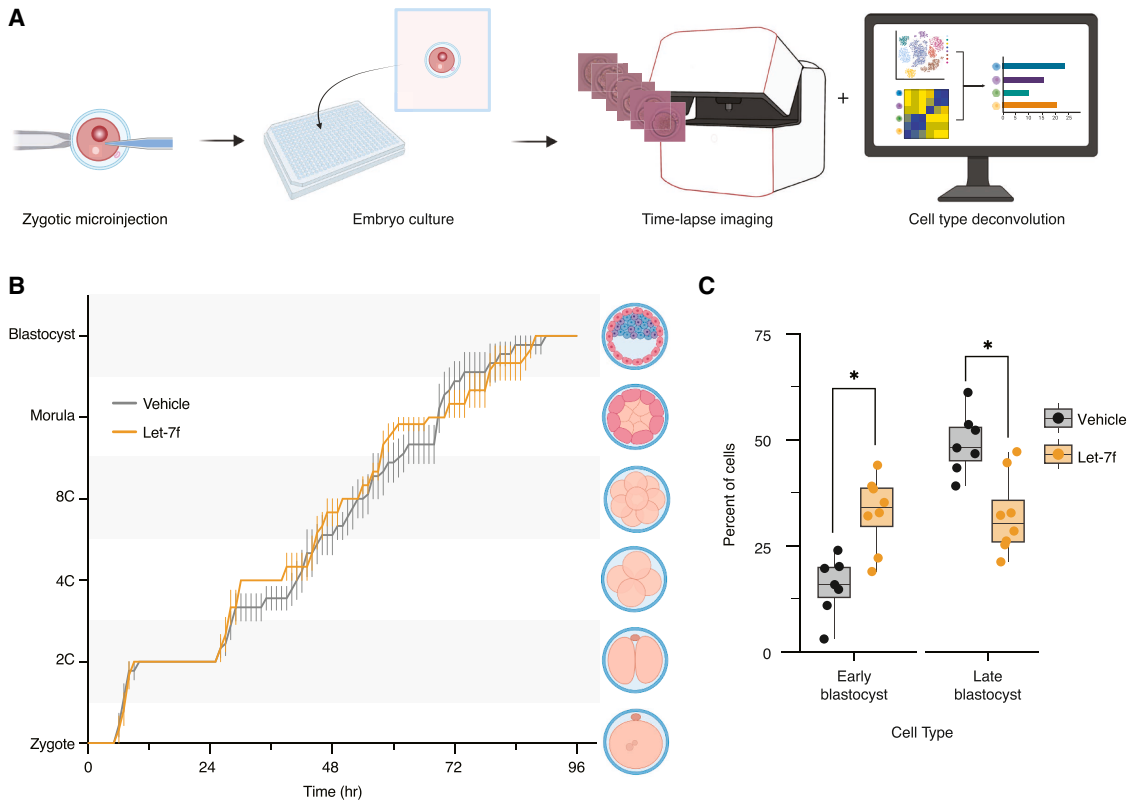

Figure 2. The trajectory of preimplantation embryo development shifted following increased zygotic let-7f

(A) Schematic representation of time-lapse imaging paradigm of preimplantation embryos (N = 20 per group) and cell type deconvolution of blastocyst RNA sequencing data.

(B) Plot visualizing transitions between main developmental stages (i.e., zygote, two-cell [2C], four-cell [4C], eight-cell [8C], morula, and blastocyst) of vehicle (N = 9) and let-7f (N = 6) embryos that successfully reached the blastocyst stage. Data are mean ± SEM.

(C) Boxplot visualizing cell type percentage for early blastocyst and late blastocyst summarized for each group as determined by cell type deconvolution. Data are median with first and third quartiles (box) and top and bottom quartiles (whiskers) indicated (Wilcoxon rank-sum tests, *FDR = 0.0184).

(A) and (B) created with BioRender.com released under a Creative Commons Attribution-NonCommercial-NoDerivs 4.0 International license (https://creativecommons.org/licenses/by-nc-nd/4.0/deed.en).

transcription and translation factors, including *Pou3f1*, *Hoxb5*, *Nkx6-2*, *Zbtb16*, and *Eif1ad6*, as well as genes that contribute to cellular metabolism, such as *Me1* and *Cbr2* (Figures 1F and 1G; Table S1).

As our RNA sequencing data showed strong evidence for the specificity of the miRNA mimic, we proceeded with only the let-7f group given its greater biological relevance.

Elevated let-7f shifts developmental rates of preimplantation embryos

To investigate if differences in developmental gene expression corresponded to changes in developmental rates, we conducted time-lapse imaging following zygotic microinjection and cell type deconvolution on our blastocyst RNA sequencing data (Figure 2A). We utilized a cumulative link mixed model to assess progression through key developmental stages (i.e., zygote, two-cell [2C], four-cell [4C], eight-cell [8C], morula, and blastocyst) based on time-lapse imaging of embryos that successfully reached the blastocyst stage (Figure 2B; Table S2). Progression over time was highly nonlinear (all spline terms $p < 0.001$). Treatment interacted significantly with time, indicating distinct developmental trajectories between vehicle and let-7f embryos. Let-7f embryos proceeded more rapidly through early cleavage stages (odds ratio $[OR]_{Spline1*treatment} = 91.9$, 95% confidence interval [CI]: 6.57–1287, $p < 0.001$; $OR_{Spline2*treatment} = 231$, 95% CI: 8.29–6409, $p = 0.0013$) but progressed significantly more slowly to later stages ($OR_{Spline5*treatment} = 5.67 \times 10^{-5}$, 95% CI: 3.1×10^{-6}–1.04×10^{-3}, $p < 0.001$) (Figure 2B; Table S2). Predicted probability curves illustrated this, with let-7f embryos predicted to more quickly reach the 2C, 4C, and 8C stages but expected to develop to the blastocyst stage more slowly (Figure S2A; Table S2).

Next, we estimated the percent of cells within our blastocysts associated with key developmental stages using a single-cell RNA sequencing reference and multi-subject single-cell deconvolution (MuSiC) (Figures 2A and S2B).[55,56] Between treatment groups, we saw a significant difference in the percent of cells mapped to the early blastocyst and late blastocyst stages

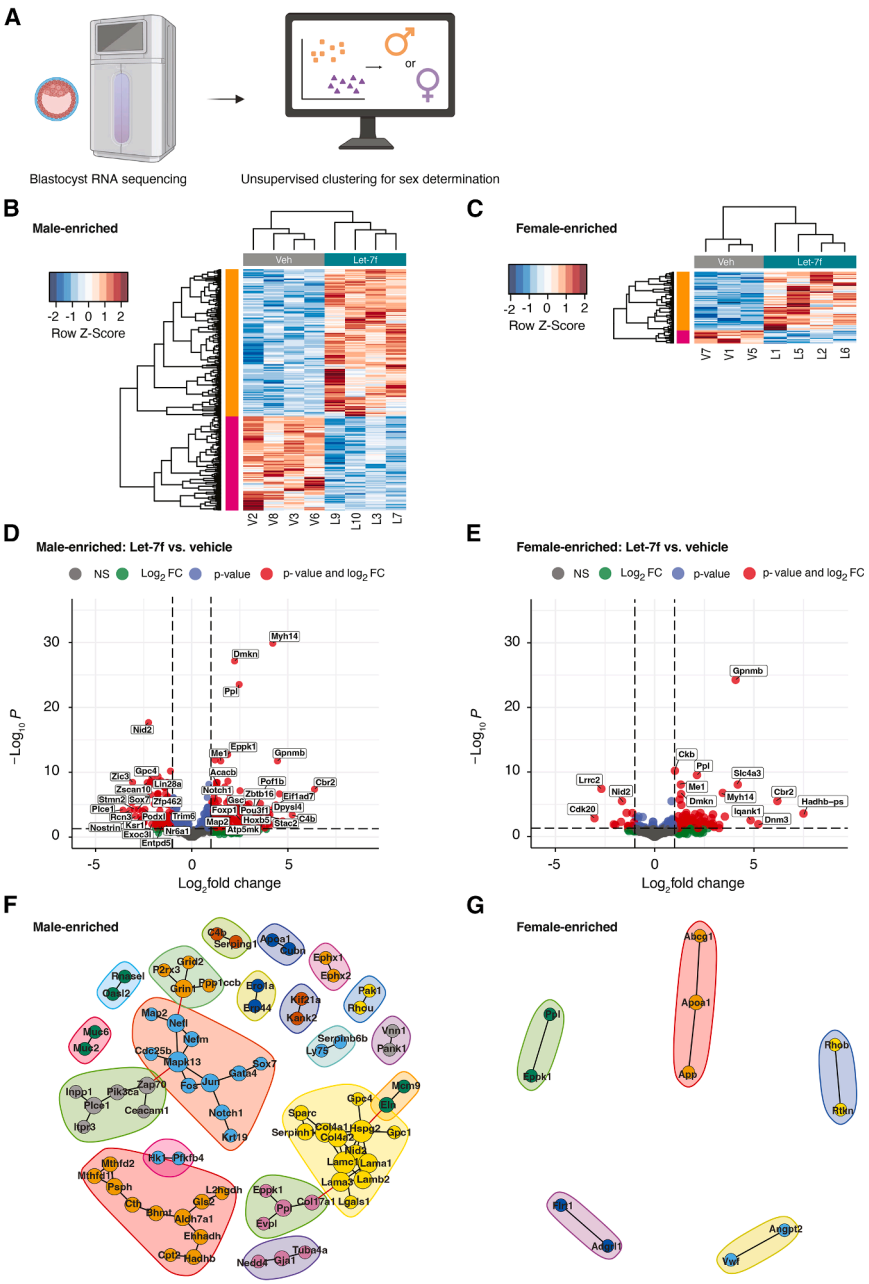

Figure 3. Let-7f altered the blastocyst transcriptome in a sex-dependent manner

(A) Schematic representation of unsupervised clustering to determine sex enrichment of pooled blastocysts used for RNA sequencing.

(B and C) Heatmaps of (B) 310 DEGs between male-enriched vehicle (N = 4 pooled) and let-7f (N = 4 pooled) blastocysts and (C) 92 DEGs between female-enriched vehicle (N = 3 pooled) and let-7f (N = 4 pooled) blastocysts. Unbiased hierarchical clustering of samples and genes are visualized by dendrogram. Orange cluster contains genes upregulated in the let-7f group, and pink cluster contains genes downregulated in the let-7f group. Vehicle samples are denoted by "V," and let-7f samples are denoted by "L".

(D and E) Volcano plots showing DEGs between (D) male-enriched let-7f and vehicle blastocysts and (E) female-enriched let-7f and vehicle blastocysts.

(F and G) PPI networks generated through STRING database for (F) male-enriched pairwise comparison and (G) female-enriched pairwise comparison, showing clustering of protein modules as determined by the Louvain method. For all, DEGs have $\log_2$ fold change $\geq |1|$ and adjusted $p \leq 0.05$.

(A) created with BioRender.com released under a Creative Commons Attribution-NonCommercial-NoDerivs 4.0 International license (https://creativecommons.org/licenses/by-nc-nd/4.0/deed.en).

(Figure 2C). Let-7f embryos had more cells mapped to the early blastocyst stage than vehicle embryos (W = 4, false discovery rate [FDR] = 0.0184) (Figure 2C). Vehicle embryos had a higher percentage of cells mapped to the late blastocyst stage (W = 51, FDR = 0.0184) (Figure 2C). These findings corresponded to our time-lapse imaging results, where let-7f embryos proceeded more slowly to the blastocyst stage (Figure 2B). Importantly, we determined that there were no significant differences in expression of key genes associated with blastocyst development (*Oct4/Pou5f1*, *Nanog*, *Cdx2*, *Sox2*, *Gata6*, *Tead4*, and *Gata3*), indicating that both groups were developmentally viable at the blastocyst stage (Table S1).[57]

Let-7f blastocyst transcriptomic differences are sex specific

To examine if the effects of increased let-7f on the blastocyst transcriptome were influenced by biological sex, we utilized unsupervised k-means clustering to define biological replicates as either "male enriched" or "female enriched" based on mean expression across all Y-linked genes (Figure 3A; Table S3). Let-7f blastocysts continued to cluster together when comparing within sex (Figures 3B and 3C). Differential gene expression analysis of male-enriched let-7f and vehicle blastocysts revealed 121 downregulated genes and 189 upregulated genes (Figure 3D; Table S4). Between female-enriched let-7f and vehicle blastocysts, we found 17 downregulated genes and 75 upregulated genes (Figure 3E; Table S4). Interestingly, there was a minimal overlap between within-sex comparisons, with let-7f male-enriched blastocysts sharing only around 10% of their DEGs with let-7f female-enriched blastocysts (Figure S3A).

To investigate the functional significance of these sex-specific transcriptomic changes, we utilized protein-protein interaction (PPI) network analysis through the STRING database. Male-enriched DEGs produced a network with 76 nodes and 78 edges with significant enrichment (p < 0.0001), suggesting a high

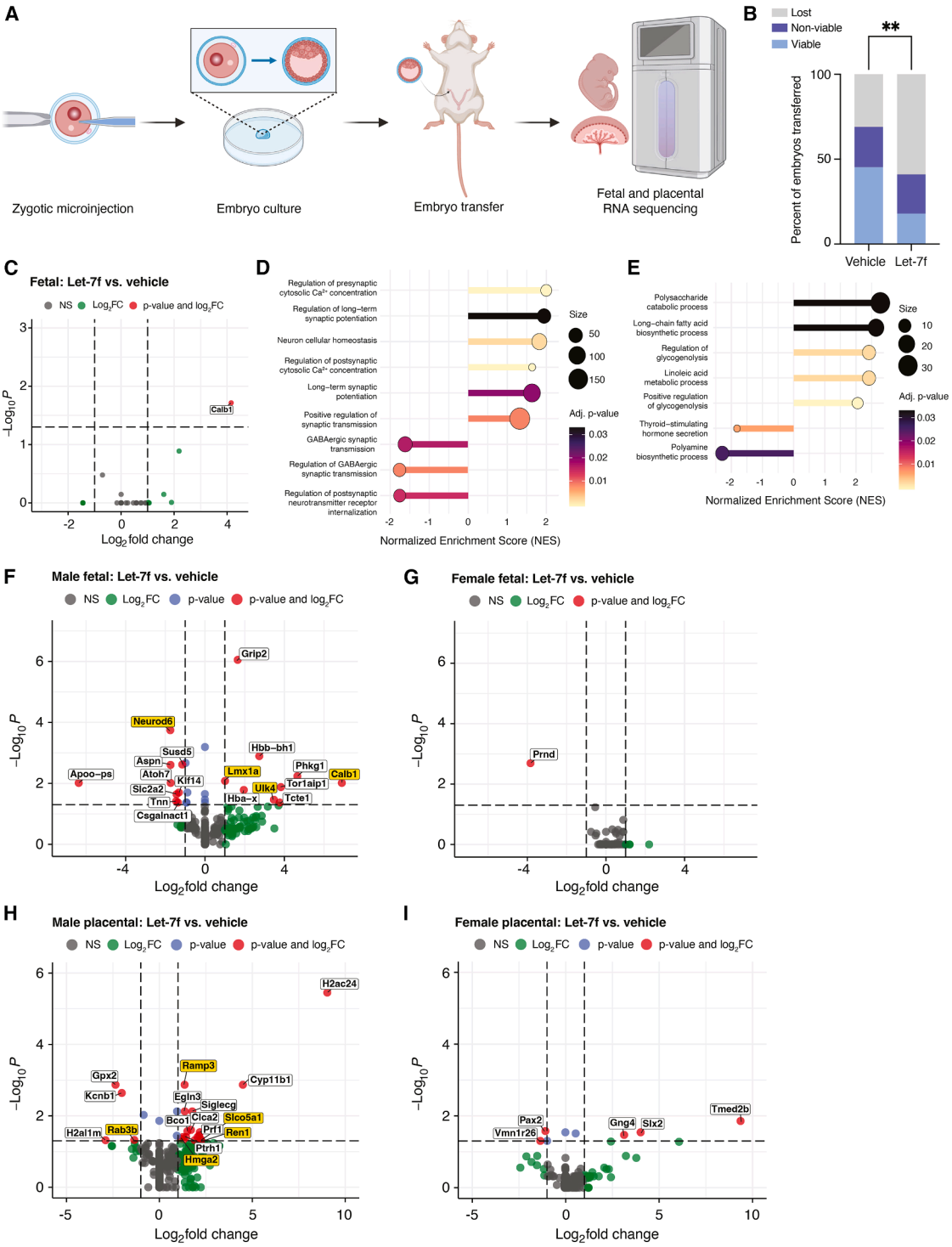

Figure 4. Transcriptomic changes caused by elevated zygotic let-7f persist to mid-gestation

(A) Schematic representation of microinjection and embryo transfer paradigm. Microinjected embryos (N = 7 per group) were transferred into recipient dams. Fetoplacental units were harvested at gestational day 12.5 (E12.5), followed by RNA isolation and sequencing.

(B) Percent of transferred embryos that resulted in viable fetuses, non-viable fetuses, or were lost at E12.5 (vehicle N = 42, let-7f N = 56; chi-square test, $^{**}p$ = 0.0065).

(C) Volcano plot showing DEGs between let-7f (N = 5) and vehicle (N = 9) fetuses.

(legend continued on next page)

degree of functional connectivity between identified proteins (Figure 3F). Using functional enrichment analysis, we determined several biological processes that were significantly overrepresented in the male-enriched PPI network. In addition to multiple developmental processes, such as tissue development and cell differentiation, we found significant enrichment for response to carbohydrates, response to glucose, and cellular glucose homeostasis (Table S5). Female-enriched DEGs generated a non-significant network with 11 nodes and 6 edges (p = 0.1835) (Figure 3G).

Transcriptomic changes persist through mid-gestation following zygotic microinjection

To determine if the influence of elevated let-7f persisted post-implantation, we transferred microinjected embryos into recipient dams and sequenced RNA from gestational day 12.5 (E12.5) fetuses and placentas (Figure 4A). There was a significant reduction in the number of viable fetuses in the let-7f group ($X^2(2)$ = 10.09, p = 0.0065) (Figure 4B). Differential gene expression analysis revealed one gene, *Calb1*, that was significantly upregulated in let-7f fetuses (Figure 4C; Table S6). We found no significant DEGs between let-7f and vehicle placentas (Figures S4A and S4B; Table S7). As we found minimal differences with differential gene expression analysis, we applied gene set enrichment analysis (GSEA) to both datasets to examine if there were pathway-level differences that would not be reflected in individual gene expression differences. GSEA revealed significant alterations in synaptic signaling and metabolic processing in our fetal gene expression data (Figures 4D and 4E; Table S6). Specifically, gene sets related to the regulation of pre- and post-synaptic calcium ion concentration, neuron cellular homeostasis, positive regulation of synaptic transmission, and regulation of glycogen catabolism were enriched in let-7f fetuses (Figures 4D and 4E). Gene sets related to GABAergic synaptic transmission and thyroid-stimulating hormone secretion were depleted in let-7f fetuses (Figures 4D and 4E). GSEA demonstrated significant enrichment in let-7f placentas for regulation of the receptor signaling pathway via JAK-STAT, steroid hormone biosynthesis, and response to corticosterone and nutrient levels (Figure S4C; Table S7).

Given the male-specific differences in the blastocyst transcriptome, we conducted within-sex comparisons on our fetal and placental RNA sequencing data. Between male fetuses, we found 9 upregulated genes, including *Grip2*, *Phkg1*, *Lmx1a*, *Ulk4*, and *Calb1*, and 9 downregulated genes, including *Neurod6*, *Aspn*, *Klf14*, *Slc2a2*, and *Tnn* (Figures 4F, S5A, and S5B). GO functional enrichment analysis on these male-specific DEGs revealed significant enrichment for neurodevelopmental processes, such as neuronal stem cell division, regulation of neuron maturation, layer formation in the cerebral cortex, and telencephalon development, within the upregulated genes (Figure S5D; Table S8). Among the downregulated genes, we found significant enrichment for other neurodevelopmental processes, including axon development and regulation of axon guidance; metabolic processes, including carbohydrate utilization and galactose and fructose transport; and bone development (Figure S5E; Table S8). Let-7f female fetuses showed significant downregulation in one gene, *Prnd* (Figures 4G and S5C). Differential gene expression analysis identified 21 DEGs between male placentas and 5 DEGs between female placentas (Figures 4H–4I, S4D, and S4E). Notably, *Ren1*, *Slco5a1*, *Bco1*, *Ptrh1*, *Egln3*, *Ramp3*, and *Hmga2* were upregulated and *Rab3b* was downregulated in male let-7f placentas (Figure 4H).

Increased zygotic let-7f alters somatic growth in a sex-specific manner

Next, we examined how these early developmental changes related to elevated let-7f influenced phenotypic differences in adult offspring (Figure 5A). Surprisingly, we found no significant differences in the percent of successful embryo transfers ($X^2(1)$ = 2.299, p = 0.13), litter sizes ($t(7)$ = 1.516, p = 0.17), gestational age at birth ($t(7)$ = 0.2659, p = 0.80), or sex ratios ($X^2(1)$ = 0.7107, p = 0.40) (Figures S6A–S6D). As let-7f was identified as dynamically responsive to prior perceived stress, we evaluated hypothalamus-pituitary-adrenal (HPA) axis responsivity. Following a brief restraint, we saw no effect of increased zygotic let-7f on male ($F_{treatment}(18)$ = 1.386, p = 0.25) or female ($F_{treatment}(18)$ = 0.0014, p = 0.97) plasma corticosterone levels (Figures S6E and S6F). We did not find an interaction of time and treatment in males ($F_{time*treatment}(33.62)$ = 0.9165, p = 0.40) or females ($F_{time*treatment}(43.81)$ = 0.26, p = 0.81) (Figures S6E and S6F). As expected, there was a main effect of time in both males ($F_{time}(33.62)$ = 267.3, p < 0.0001) and females ($F_{time}(43.81)$ = 333.7, p < 0.0001) (Figures S6E and S6F).

To evaluate overall growth and development, we assessed body weight from 3 to 8 weeks old. There was no overall difference between vehicle and let-7f males (β = 0.42 ± 0.89, t = 0.47, p = 0.64), but a significant interaction between treatment group and week was found, specifically at 6 weeks (β = 1.15 ± 0.54, t = 2.12, p = 0.035), 7 weeks (β = 1.22 ± 0.54, t = 2.26, p = 0.025), and 8 weeks (β = 1.80 ± 0.54, t = 3.33, p = 0.0011), indicating that the temporal trajectory differed between groups (Figure 5B). When comparing body weights at 8 weeks, let-7f males weighed significantly more than vehicle males ($t(28)$ = 2.055, p = 0.049). Let-7f males also gained significantly more weight overall compared to vehicle males ($t(28)$ = 2.046, p = 0.05) (Figures 5B and 5C). Conversely, no differences were found when comparing vehicle and let-7f female offspring in body

(D and E) Gene sets significantly altered in E12.5 fetuses as determined by GSEA were related to (D) synaptic signaling and (E) metabolic processing. Positive normalized enrichment score (NES) corresponds to enrichment in the let-7f group, and negative NES corresponds to enrichment in the vehicle group.
(F and G) Volcano plots showing DEGs between (F) male let-7f (N = 2) and vehicle (N = 4) fetuses and (G) female let-7f (N = 3) and vehicle (N = 5) fetuses. Notable DEGs are highlighted in yellow in (F).
(H and I) Volcano plots showing DEGs between (H) male let-7f (N = 3) and vehicle (N = 5) placentas and (I) female let-7f (N = 6) and vehicle (N = 4) placentas. Notable DEGs are highlighted in yellow in (H). For all, DEGs have $\log_2$ fold change $\geq |1|$ and adjusted $p \leq 0.05$.

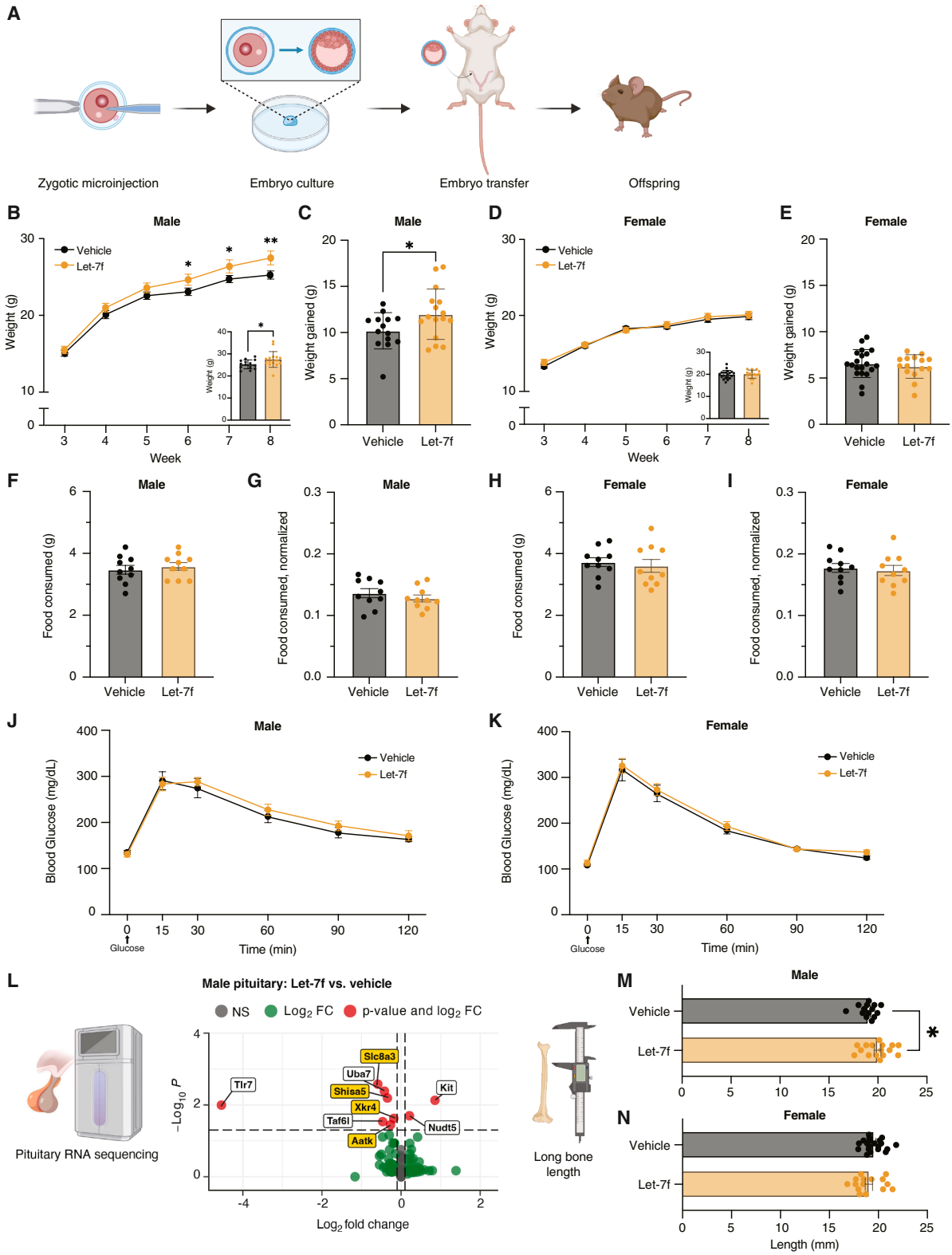

Figure 5. Male let-7f offspring had increased weight gain, differential pituitary gene expression, and greater long bone length

(A) Schematic representation of microinjection and embryo transfer paradigm. Microinjected embryos (N = 10–15) were transferred into recipient dams, and offspring were followed into adulthood.

(legend continued on next page)

weight trajectory ($F_{treatment}(33) = 0.1745$, $p = 0.68$; $F_{time*treatment}(81.08) = 0.90$, $p = 0.43$) (Figure 5D). We also saw no differences between vehicle and let-7f females in body weight at 8 weeks ($t(33) = 0.2937$, $p = 0.77$) or overall weight gain ($t(33) = 0.6574$, $p = 0.52$) (Figures 5D and 5E). Both males and females showed a strong effect of time on body weight ($p < 0.0001$) (Figures 5B and 5D). To examine underlying factors that may contribute to this male-specific increase in weight gain, we quantified food consumption over a 24-h period. We found no differences among male or female offspring in food consumption in grams ($t(18) = 0.5855$, $p = 0.57$; $t(18) = 0.4712$, $p = 0.64$) or when normalized to body weight ($t(18) = 0.9209$, $p = 0.37$; $t(18) = 0.3797$, $p = 0.71$) (Figures 5F–5I). Next, we conducted a glucose tolerance test to investigate any changes in glucose homeostasis. We did not observe a significant effect of treatment ($F_{treatment}(18) = 0.3518$, $p = 0.56$; $F_{treatment}(18) = 0.56$, $p = 0.46$) or an interaction of time and treatment ($F_{time*treatment}(51.70) = 0.3941$, $p = 0.75$; $F_{time*treatment}(34.39) = 0.0899$, $p = 0.91$) on blood glucose levels in males or females (Figures 5J and 5K). As expected, both males and females showed a significant main effect of time on blood glucose levels ($F_{time}(51.70) = 53.95$, $p < 0.0001$); $F_{time}(34.39) = 110.5$, $p < 0.0001$) (Figures 5J and 5K).

We next investigated potential endocrine contributors in male offspring, specifically gene expression changes in the pituitary gland. We found 2 upregulated and 7 downregulated genes, including *Tlr7*, *Xkr4*, *Shisa5*, *Slc8a3*, and *Aatk* (Figure 5L; Table S9). To determine whether increased body weight and gene expression changes in the pituitary corresponded with altered linear growth, we measured long bone (i.e., tibia) length postmortem. We observed significantly greater tibia length in let-7f male offspring ($t(28) = 2.224$, $p = 0.03$) (Figure 5M). Tibia length was not significantly different between female offspring ($t(33) = 1.183$, $p = 0.25$) (Figure 5N).

DISCUSSION

The developmental origins of health and disease (DOHaD) suggest that early life exposures, including those during the preconception window, can have a lasting impact on disease risk throughout life.[58] While much of this field has focused on maternal experiences, the paternal preconception environment, including that of prior stress and trauma, has gained increased attention for important contributions to offspring developmental plasticity transferred at conception.[7,13–15,27–30,32,33,59] Sperm small non-coding RNAs (sncRNAs), including miRNAs, serve as environmentally responsive signals positioned to ''transmit'' paternal experiences at fertilization. However, we still know little as to how changes in levels of specific sperm miRNAs alter offspring development. In a longitudinal human cohort, we previously identified the miRNA, let-7f, as statistically significantly elevated in response to subject's prior perceived stress. The let-7 miRNA family is highly conserved across species and known to play endogenous roles in reproductive processes and in embryo development.[43–50] Therefore, we examined the developmental effects of elevated let-7f post-fertilization.

First, to validate our zygotic microinjection approach, we utilized 2 let-7f miRNA mimic concentrations compared to a vehicle injection to determine changes to early embryonic developmental progression. Both let-7f and 2× let-7f microinjections produced embryos that successfully reached the blastocyst stage but at a reduced rate. Previous studies similarly reported that differential expression of let-7 isoforms in human sperm and in early embryos corresponded with changes in blastulation rates, supporting a role for let-7f that may predict cell differentiation and embryo survival.[47,48,50] Next, utilizing RNA sequencing at the blastocyst stage, we validated the specificity of our let-7f mimic microinjections by demonstrating that both concentrations produced similar patterns of gene expression changes compared to vehicle. Unbiased hierarchical clustering distinguished both let-7f and 2× let-7f from vehicle blastocysts, supporting a specificity of let-7f for maternal mRNA targets in the zygote and resulting outcomes by the blastocyst stage. GO functional enrichment analyses of these blastocysts revealed overrepresentation of cellular and developmental processes important for embryogenesis among shared DEGs.

In the examination of statistically significantly altered blastocyst gene expression, both let-7f concentrations altered the same genes and in the same direction, again supporting the specificity of initial targeting of the let-7f mimic. Furthermore, we found an overlap between downregulated DEGs and predicted let-7f targets, suggesting canonical let-7f activity of the mimic. Interestingly, however, most downregulated genes did not overlap with predicted let-7f targets, and we found a greater number of upregulated genes. Post-fertilization, miRNAs selectively target stored maternal mRNA for degradation through the RNA-induced silencing complex (RISC) to facilitate the

(B) Weekly body weights from 3 to 8 weeks in males ($N = 14–16$ per group; linear mixed-effects model). Let-7f males were significantly heavier at 6 weeks ($^*p = 0.035$), 7 weeks ($^*p = 0.025$), and 8 weeks ($^{**}p = 0.0011$). Final body weight at 8 weeks is shown by bar graph (unpaired two-tailed Student's *t* tests, $^*p = 0.049$).
(C) Total weight gained from 3 to 8 weeks in males (unpaired two-tailed Student's t tests, $^*p = 0.05$).
(D) Weekly body weights from 3 to 8 weeks in females ($N = 15–20$ per group). Final body weight at 8 weeks is shown by bar graph.
(E) Total weight gained from 3 to 8 weeks in females.
(F and G) 24-h food consumption of male offspring ($N = 10$ per group) (F) in grams and (G) normalized to individual body weight.
(H and I) 24-h food consumption of female offspring ($N = 10$ per group) (H) in grams and (I) normalized to individual body weight.
(J and K) Blood glucose levels during a glucose tolerance test in (J) male offspring ($N = 10$ per group) and (K) female offspring ($N = 10$ per group).
(L) Volcano plot showing DEGs between male let-7f and vehicle pituitary glands ($N = 6$ per group). DEGs have $\log_2$ fold change $\geq |0.1|$ and adjusted $p \leq 0.05$. Notable DEGs are highlighted in yellow.
(M) Long bone (tibia) length in male offspring ($N = 14–16$ per group; unpaired two-tailed Student's *t* tests, $^*p = 0.03$).
(N) Long bone (tibia) length in female offspring ($N = 15–20$ per group).
(A) and graphics for (L), (M), and (N) created with BioRender.com released under a Creative Commons Attribution-NonCommercial-NoDerivs 4.0 International license (https://creativecommons.org/licenses/by-nc-nd/4.0/deed.en).
All data presented are mean ± SEM.

maternal-to-zygotic transition (MZT).[38,60–64] With an expected half-life of ~19 h, we surmise that let-7f's main direct actions are within the zygote, likely targeting maternal mRNA for degradation and impacting zygotic genome activation (ZGA).[65] Thus, at the blastocyst stage, we primarily capture downstream changes resulting from earlier let-7f action in the zygote, with some direct effects persisting.

Notably, propagation of changes resulting from both concentrations of zygotic let-7f microinjections increased expression of metabolic enzymes, malic enzyme 1 (ME1) and carbonyl reductase 2 (CBR2), by the blastocyst stage. ME1 functions cytosolically to convert malate to pyruvate and generate NADPH, and CBR2 is localized to mitochondria, playing a role in glucose metabolism.[66–69] Upregulation of these genes suggests a potential increase in the metabolic demands of let-7f embryos. During the later stages of preimplantation development, embryos undergo compaction, cavitation, and cellular differentiation, resulting in the ICM that gives rise to the embryo-proper and the TE that contributes to the placenta.[70–72] These processes are metabolically demanding, and changes in metabolic functioning may reflect a shift in the rate of vital developmental transitions.[73] For example, we found that important regulators involved in balancing pluripotency and differentiation, *Lin28a*, *Trim6*, *Zic3*, and *Sox7*, were downregulated in let-7f blastocysts, again suggesting a potential deviation from expected embryonic progression.[74–79]

Next, to assess how increased zygotic let-7f at the stress-relevant concentration impacted the rate of preimplantation embryo development, we used time-lapse imaging to measure embryo transition rates. For embryos that successfully developed into blastocysts, we found that let-7f embryos initially proceeded at an accelerated rate but then transitioned more slowly between the morula and blastocyst stages. Cell type deconvolution of our blastocyst RNA sequencing confirmed this delayed progression to the blastocyst stage, as a greater percentage of let-7f blastomeres was classified as early blastocyst compared to vehicle and fewer as late blastocyst. Our results, along with previous findings in humans, suggest that increased let-7f at the zygote stage is designed to accelerate development, but this faster progression may not be ultimately supported by the embryo, resulting in let-7f embryos arresting before the blastocyst stage and slowed development for embryos that proceed.[43,47–49,80,81] Let-7f embryos that did reach the blastocyst stage were developmentally viable as we found no differences in key transcription factors associated with blastocyst development. We found that transcriptomic changes in let-7f blastocysts were related to metabolism and cellular differentiation, highlighting that disruptions in these pathways likely contributed to differences in developmental rate.[82,83]

Given the critical importance of biological sex in embryo development and that the mature miRNA, mmu-let-7f-5p, is, in part, derived from the X chromosome, we also examined the influence of sex on let-7f-induced changes in the blastocyst transcriptome.[43,84] With unsupervised *k*-means clustering, we categorized our pooled blastocyst samples as either male or female enriched and analyzed differences in gene expression within sex. Let-7f male-enriched blastocysts showed 3× as many DEGs as female-enriched samples. Importantly, the process of X chromosome inactivation is incomplete during preimplantation development, contributing to distinct gene expression patterns between male and female embryos.[85–87] Additionally, *let-7f-2*, one of the precursor genes of let-7f, is encoded on the X chromosome, suggesting possible sex differences in the regulation of let-7f.[43,84] Therefore, there are likely skewed differences in gene targets and regulatory processes that have facilitated a male-specific action of elevated let-7f post-fertilization. Next, to gain biological insight into the sex-specific blastocyst DEGs, we utilized PPI network analysis through the STRING database. Notably, male-specific DEGs generated a strong PPI network functionally enriched for developmental and metabolic processes, including response to glucose and cellular glucose homeostasis. Female-specific DEGs, however, failed to generate a significant PPI network. In addition to its role in energy production, glucose plays an important role in the embryo transition from morula to blastocyst. Around this stage, a metabolic switch occurs where glucose is essential for embryo development, specifically for TE differentiation.[82,88–90]

To further investigate the influence of increased zygotic let-7f on embryo ICM and TE lineages, we examined fetal and placental development at mid-gestation using transcriptomic changes as a proxy for effects of zygote microinjection. We confirmed that let-7f embryos were capable of successfully implanting and developing into morphologically normal fetoplacental units. However, similar to our preimplantation results, we found a reduction in the percent of let-7f embryos that resulted in viable fetuses. GSEA revealed significant transcriptomic changes related to neuronal and metabolic function in let-7f fetuses. Fetal metabolism is closely linked with neurodevelopment, and disruptions of metabolic processing during this time have been associated with increased risk for neurodevelopmental disorders in human studies.[91–94] GSEA also indicated that let-7f placentas had altered gene expression that was related to a response to nutrient levels. At the interface of the maternal and fetal environment, the placenta is also critical in supporting and regulating fetal metabolism and subsequent development.[91,95,96]

Given the sex differences identified in the blastocyst transcriptome, we also investigated sex differences in our fetal and placental gene expression data. Remarkably, we again found a greater number of DEGs in the male let-7f fetus and placenta compared to very little changes detected within female comparisons. GO functional enrichment analysis identified transcriptional changes related to neurodevelopment, metabolism, and skeletal development in male let-7f fetuses. Genes identified in let-7f male fetuses included *Calb1*, *Neurod6*, *Lmx1a*, and *Ulk4*, crucial for neuronal differentiation and development.[97–100] *Calb1* was also identified as the only DEG when comparing let-7f to vehicle fetuses.

Interestingly, *Calb1* is a focus of neurodevelopment studies in humans and found to be a key regulator of brain development and function, primarily by controlling intracellular calcium dynamics and acting as a marker for mature neurons.[101,102] Its proper expression is crucial for synaptic plasticity, learning, and memory, and dysregulation is associated with several neurodevelopmental and neurodegenerative disorders, including a risk for autism spectrum disorder.[103–105] Further, *Calb1* also plays a crucial, complex role in bone formation, acting as a

calcium buffer in osteoblasts and osteocytes, and in regulating bone remodeling.[106]

In placental tissue, within-male comparisons revealed genes important for maternal-fetal circulation and placental growth, including *Ren1*, *Slco5a1*, *Ramp3*, *Rab3b*, and *Hmga2*, in let-7f males.[107–112] Not surprisingly, changes in placental function and development are associated with disease susceptibility, including cardiometabolic and neuropsychiatric disorders.[113] Thus, alterations in placental circulation may contribute to the neurodevelopmental and metabolic transcriptomic changes found in let-7f fetuses.

To determine if the developmental differences we identified corresponded with an offspring phenotype, we compared adult male and female mice following zygotic let-7f microinjection. We found that let-7f embryos developed into healthy offspring with no significant differences in embryo transfer rates, litter sizes, gestational age at birth, or sex ratios. As a measure of overall health, we examined offspring growth rates using body weight trajectory from 3 to 8 weeks of age. We found that let-7f males, but not females, were significantly heavier starting at 6 weeks and gained significantly more weight overall. First, we examined food intake and glucose homeostasis in adult mice as a possible cause of increased weight gain but found no differences for either let-7f males or females. We also evaluated homeostatic regulation by comparing male and female HPA stress axis responsivity to an acute restraint as we have previously demonstrated in mice that paternal stress produced offspring with a hyporesponsive HPA.[28,29,64] However, we found no differences in corticosterone baseline, stress maximal rise, or stress recovery in the HPA axis for either male or female let-7f mice.

Given that differences in let-7f male body weights seemed to diverge around the onset of puberty, we further investigated potential endocrine contributors. With fetal transcriptomic differences identified as neurodevelopmental and as the hypothalamus-pituitary axis is a key regulator of growth, sex hormone production, and metabolic rate, we conducted RNA sequencing of male pituitary glands as a proxy for potential differences in endocrine function between the brain and periphery.[114] As we investigated these transcriptomic differences months after the initial microinjection at the zygote stage, we hypothesized that we would find subtle differences in gene expression that would indicate a shift in developmental trajectory. To capture these differences, we utilized a $\log_2$ fold change threshold $\geq$0.1. Interestingly, *Tlr7*, a critical immune receptor expressed in dendritic cells, was significantly downregulated in the let-7f male pituitary.[115] Dendritic cells in the pituitary regulate the growth and function of hormone-producing cells, including corticotropes and gonadotrophs, suggesting a potential alteration in these cell populations in let-7f males.[116,117] However, we did not see differences in corticosterone production in response to stress in males. Immune challenges were not examined here but could be a focus of future studies in this model.

In further examination of the genes significantly altered in the pituitary, we found several significantly downregulated genes in let-7f males, *Slc8a3*, *Shisa5*, *Xkr4*, and *Aatk*, that shared similar associations with traits from human genome-wide association studies (GWASs). Genetic variations of these genes, especially *Slc8a3* and *Xkr4*, are linked to bone tissue density, body height, and signaling pathways vital for skeletal growth.[118–124] Therefore, as we found that the let-7f males weighed more following puberty but did not detect differences in food intake or glucose metabolism, we next investigated whether osteogenesis was impacted by measuring tibia length in these mice. Indeed, we found that only let-7f males had significantly increased long bone length. While exciting, our findings do not exclude additional pubertal differences that may contribute to changes in somatic growth in let-7f male offspring, and given that these mice were on a nutritious, high-fiber diet, studies examining a high-fat, low-fiber diet may identify additional metabolic differences in let-7f mice.[125]

In summary, we replicated increased sperm let-7f levels using zygotic microinjection and identified male-specific developmental changes in gene expression throughout embryo and fetal development, with increased body weight and bone length in adult male offspring. Significant transcriptional alterations related to metabolism, neurodevelopment, bone growth, and a wide range of developmental processes suggest an early mechanism contributing to the adult phenotype presentation, but future studies are necessary to interrogate the mechanisms underlying the precise developmental action of elevated let-7f. Importantly, we are not suggesting that the let-7f mimic is continuously and directly regulating gene expression across cell divisions and development, but rather that the gene expression changes we detect at each stage represent a response to, and consequence of, earlier let-7f action. Certainly, the phenotype of increased body weight and bone length in let-7f male mice may be a consequence of an overall effect of increased let-7f on embryo developmental rates.[126–128] Our current findings provide important insights into embryonic mechanisms that may facilitate developmental plasticity, enhancing our understanding of paternal epigenetic inheritance.

Limitations of the study

We recognize the limitation that let-7f was only one of the miRNAs identified in our prior human sperm study and that coordination between several dynamic sncRNA may result in changes occurring at fertilization that drive unique developmental outcomes. Our study also utilized two concentrations of the let-7f mimic as well as a vehicle microinjection control to validate specificity of the mimic and to control for embryo handling and injection. As chemistry-matched non-targeting (scrambled) mimic controls are still loaded into the cell's RISC complex, producing off-target effects, we instead included a second mimic concentration as a specificity comparison.[129] Our findings demonstrating a sex-specific effect of let-7f on blastocyst outcomes were based on comparisons of sex-enriched pooled samples, identified by enrichment of Y chromosome genes. Future studies could examine RNA sequencing of embryos at earlier stages or individual blastocysts. Analysis of transcriptomic differences in male let-7f fetuses is also limited by the small number of biological replicates. While we limited our investigation of pituitary gene expression to male offspring only, future studies could conduct a more exhaustive evaluation of endocrine-related differences in both male and female adult animals. Finally, future work is needed to verify the

mechanistic actions of gene expression changes on adult phenotypes.

RESOURCE AVAILABILITY

Lead contact

Requests for further information and resources should be directed to and will be fulfilled by the lead contact, Dr. Tracy L. Bale (tracy.bale@cuanschutz.edu).

Materials availability

This study did not generate new unique reagents.

Data and code availability

- Bulk RNA sequencing data have been deposited at the Gene Expression Omnibus repository as GEO: GSE314398, GSE314467, GSE314710, and GSE314713 and are publicly available as of the date of publication.
- This paper does not report original code.
- Any additional information required to reanalyze the data reported in this paper is available from the lead contact upon request.

ACKNOWLEDGMENTS

We thank the University of Colorado Anschutz Genomics Shared Resource Core (RRID: SCR_021984) for help with our RNA sequencing and Jessica Fluharty for technical assistance. This work was supported by the National Institutes of Health grants: MH129495 (T.L.B.), HD097093 (T.L.B.), MH108286 (T.L.B.), and HD105771 (T.L.B. and C.N.E.).

AUTHOR CONTRIBUTIONS

Conceptualization, A.C.J. and T.L.B.; methodology, A.C.J., K.C.C., N.M., N.A.L., and T.L.B.; software, A.C.J., A.S.F., and N.M.; formal analysis, A.C.J. and A.S.F.; investigation, A.C.J., K.C.C., and N.A.L.; writing – original draft, A.C.J. and T.L.B.; review and editing, A.C.J., K.C.C., N.M., C.N.E., and T.L.B.; funding acquisition, T.L.B. and C.N.E.

DECLARATION OF INTERESTS

The authors declare no competing interests.

STAR★METHODS

Detailed methods are provided in the online version of this paper and include the following:

- KEY RESOURCES TABLE
- EXPERIMENTAL MODEL AND STUDY PARTICIPANT DETAILS
  - Study approval
  - Embryo microinjections
  - Embryo culture and transfer
- METHOD DETAILS
  - RNA isolation and library prep of blastocysts
  - RNA isolation and library prep of E12.5 tissues
  - RNA isolation and library prep of adult pituitary glands
  - Time-lapse imaging of preimplantation embryos
  - Hypothalamus-pituitary-adrenal (HPA) axis assessment
  - 24-h food consumption
  - Glucose tolerance test
- QUANTIFICATION AND STATISTICAL ANALYSIS
  - RNA sequencing analyses
  - Time-lapse imaging analysis
  - Additional analyses

SUPPLEMENTAL INFORMATION

Supplemental information can be found online at https://doi.org/10.1016/j.isci.2026.116115.

Received: January 9, 2026
Revised: January 15, 2026
Accepted: May 11, 2026
Published: May 26, 2026

REFERENCES

1. Huang, C., Li, Z., Narayan, K.M., Williamson, D.F., and Martorell, R. (2010). Bigger babies born to women survivors of the 1959-1961 Chinese famine: a puzzle due to survival selection? Journal of Developmental Origins of Health and Disease *1*, 412–418. https://doi.org/10.1017/s2040174410000504.
2. Stein, A.D., Pierik, F.H., Verrips, G.H., Susser, E.S., and Lumey, L.H. (2009). Maternal exposure to the Dutch famine before conception and during pregnancy: quality of life and depressive symptoms in adult offspring. Epidemiology *20*, 909–915. https://doi.org/10.1097/EDE.0b013e3181b5f227.
3. Soubry, A., Murphy, S.K., Wang, F., Huang, Z., Vidal, A.C., Fuemmeler, B.F., Kurtzberg, J., Murtha, A., Jirtle, R.L., Schildkraut, J.M., and Hoyo, C. (2015). Newborns of obese parents have altered DNA methylation patterns at imprinted genes. Int. J. Obes. *39*, 650–657. https://doi.org/10.1038/ijo.2013.193.
4. Hultman, C.M., Sandin, S., Levine, S.Z., Lichtenstein, P., and Reichenberg, A. (2011). Advancing paternal age and risk of autism: new evidence from a population-based study and a meta-analysis of epidemiological studies. Mol. Psychiatr. *16*, 1203–1212. https://doi.org/10.1038/mp.2010.121.
5. Janecka, M., Haworth, C.M.A., Ronald, A., Krapohl, E., Happé, F., Mill, J., Schalkwyk, L.C., Fernandes, C., Reichenberg, A., and Rijsdijk, F. (2017). Paternal Age Alters Social Development in Offspring. Journal of the American Academy of Child and Adolescent Psychiatry *56*, 383–390. https://doi.org/10.1016/j.jaac.2017.02.006.
6. Uldbjerg, C.S., Leader, J., Minguez-Alarcon, L., Chagnon, O., Dadd, R., Ford, J., Fleury, E., Williams, P., Juul, A., Bellinger, D.C., et al. (2024). Associations of maternal and paternal preconception and maternal pregnancy urinary phthalate biomarker and bisphenol A concentrations with offspring autistic behaviors: The PEACE study. Environ. Res. *263*, 120253. https://doi.org/10.1016/j.envres.2024.120253.
7. Costa, D.L., Yetter, N., and DeSomer, H. (2018). Intergenerational transmission of paternal trauma among US Civil War ex-POWs. Proc. Natl. Acad. Sci. USA *115*, 11215–11220. https://doi.org/10.1073/pnas.1803630115.
8. Svanes, C., Koplin, J., Skulstad, S.M., Johannessen, A., Bertelsen, R.J., Benediktsdottir, B., Bråbäck, L., Elie Carsin, A., Dharmage, S., Dratva, J., et al. (2017). Father's environment before conception and asthma risk in his children: a multi-generation analysis of the Respiratory Health In Northern Europe study. Int. J. Epidemiol. *46*, 235–245. https://doi.org/10.1093/ije/dyw151.
9. Fleming, T.P., Watkins, A.J., Velazquez, M.A., Mathers, J.C., Prentice, A.M., Stephenson, J., Barker, M., Saffery, R., Yajnik, C.S., Eckert, J.J., et al. (2018). Origins of lifetime health around the time of conception: causes and consequences. Lancet *391*, 1842–1852. https://doi.org/10.1016/s0140-6736(18)30312-x.
10. Ramirez, D., and Haas, S.A. (2022). Windows of Vulnerability: Consequences of Exposure Timing during the Dutch Hunger Winter. Popul. Dev. Rev. *48*, 959–989. https://doi.org/10.1111/padr.12513.
11. Pembrey, M.E., Bygren, L.O., Kaati, G., Edvinsson, S., Northstone, K., Sjöström, M., and Golding, J. (2006). Sex-specific, male-line transgenerational responses in humans. Eur. J. Hum. Genet. *14*, 159–166. https://doi.org/10.1038/sj.ejhg.5201538.

12. Kaati, G., Bygren, L.O., and Edvinsson, S. (2002). Cardiovascular and diabetes mortality determined by nutrition during parents' and grandparents' slow growth period. Eur. J. Hum. Genet. *10*, 682–688. https://doi.org/10.1038/sj.ejhg.5200859.

13. Jawaid, A., Jehle, K.-L., and Mansuy, I.M. (2021). Impact of Parental Exposure on Offspring Health in Humans. Trends Genet. *37*, 373–388. https://doi.org/10.1016/j.tig.2020.10.006.

14. Chan, J.C., Nugent, B.M., and Bale, T.L. (2018). Parental Advisory: Maternal and Paternal Stress Can Impact Offspring Neurodevelopment. Biol. Psychiatry *83*, 886–894. https://doi.org/10.1016/j.biopsych.2017.10.005.

15. Yehuda, R., Daskalakis, N.P., Bierer, L.M., Bader, H.N., Klengel, T., Holsboer, F., and Binder, E.B. (2016). Holocaust Exposure Induced Intergenerational Effects on FKBP5 Methylation. Biol. Psychiatry *80*, 372–380. https://doi.org/10.1016/j.biopsych.2015.08.005.

16. Brumberg, H.L., and Shah, S.I. (2020). Got daddy issues? Fathers impact on perinatal outcomes. Semin. Perinatol. *44*, 151238. https://doi.org/10.1016/j.semperi.2020.151238.

17. Chen, E., da Cruz, R.S., Nascimento, A., Joshi, M., Pereira, D.G., Dominguez, O., Fernandes, G., Smith, M., Paiva, S.P.C., and de Assis, S. (2024). Paternal DDT exposure induces sex-specific programming of fetal growth, placenta development and offspring's health phenotypes in a mouse model. Sci. Rep. *14*, 7567. https://doi.org/10.1038/s41598-024-58176-7.

18. Conner, K.E., Bottom, R.T., and Huffman, K.J. (2020). The Impact of Paternal Alcohol Consumption on Offspring Brain and Behavioral Development. Alcohol Clin. Exp. Res. *44*, 125–140. https://doi.org/10.1111/acer.14245.

19. Goli, P., Yazdi, M., Poursafa, P., and Kelishadi, R. (2021). Intergenerational influence of paternal physical activity on the offspring's brain: A systematic review and meta-analysis. Int. J. Dev. Neurosci. *81*, 10–25. https://doi.org/10.1002/jdn.10081.

20. Hernandez, R., Li, X., Shi, J., Dave, T.R., Zhou, T., Chen, Q., and Zhou, C. (2024). Paternal hypercholesterolemia elicits sex-specific exacerbation of atherosclerosis in offspring. JCI Insight *9*, e179291. https://doi.org/10.1172/jci.insight.179291.

21. Li, J., Tsuprykov, O., Yang, X., and Hocher, B. (2016). Paternal programming of offspring cardiometabolic diseases in later life. J. Hypertens. *34*, 2111–2126. https://doi.org/10.1097/hjh.0000000000001051.

22. Luan, M., Zhang, X., Fang, G., Liang, H., Yang, F., Song, X., Chen, Y., Yuan, W., and Miao, M. (2022). Preconceptional paternal alcohol consumption and the risk of child behavioral problems: a prospective cohort study. Sci. Rep. *12*, 1508. https://doi.org/10.1038/s41598-022-05611-2.

23. Mao, Y., Zhao, Y., Luo, S., Chen, H., Liu, X., Wu, T., Ding, G., Liu, X., Sheng, J., Meng, Y., and Huang, H. (2022). Advanced paternal age increased metabolic risks in mice offspring. Biochim. Biophys. Acta Mol. Basis Dis. *1868*, 166355. https://doi.org/10.1016/j.bbadis.2022.166355.

24. Veldkamp, S.A.M., Zondervan-Zwijnenburg, M.A.J., van Bergen, E., Barzeva, S.A., Tamayo-Martinez, N., Becht, A.I., van Beijsterveldt, C.E.M., Meeus, W., Branje, S., Hillegers, M.H.J., et al. (2021). Parental Age in Relation to Offspring's Neurodevelopment. J. Clin. Child Adolesc. Psychol. *50*, 632–644. https://doi.org/10.1080/15374416.2020.1756298.

25. Watkins, A.J., Rubini, E., Hosier, E.D., and Morgan, H.L. (2020). Paternal programming of offspring health. Early Hum. Dev. *150*, 105185. https://doi.org/10.1016/j.earlhumdev.2020.105185.

26. Shi, Q., and Qi, K. (2023). Developmental origins of health and disease: Impact of paternal nutrition and lifestyle. Pediatric Investigation *7*, 111–131. https://doi.org/10.1002/ped4.12367.

27. Saavedra-Rodríguez, L., and Feig, L.A. (2013). Chronic Social Instability Induces Anxiety and Defective Social Interactions Across Generations. Biol. Psychiatry *73*, 44–53. https://doi.org/10.1016/j.biopsych.2012.06.035.

28. Rodgers, A.B., Morgan, C.P., Bronson, S.L., Revello, S., and Bale, T.L. (2013). Paternal Stress Exposure Alters Sperm MicroRNA Content and Reprograms Offspring HPA Stress Axis Regulation. J. Neurosci. *33*, 9003–9012. https://doi.org/10.1523/jneurosci.0914-13.2013.

29. Chan, J.C., Morgan, C.P., Adrian Leu, N., Shetty, A., Cisse, Y.M., Nugent, B.M., Morrison, K.E., Jašarević, E., Huang, W., Kanyuch, N., et al. (2020). Reproductive tract extracellular vesicles are sufficient to transmit intergenerational stress and program neurodevelopment. Nat. Commun. *11*, 1499. https://doi.org/10.1038/s41467-020-15305-w.

30. Dietz, D.M., LaPlant, Q., Watts, E.L., Hodes, G.E., Russo, S.J., Feng, J., Oosting, R.S., Vialou, V., and Nestler, E.J. (2011). Paternal Transmission of Stress-Induced Pathologies. Biol. Psychiatry *70*, 408–414. https://doi.org/10.1016/j.biopsych.2011.05.005.

31. Kleeman, E.A., Gubert, C., Reisinger, S.N., Davidson, K.C., Lu, D., Dayton, M., Mackiewicz, L., Masson, B.A., Adithya, P., Garnham, A.L., et al. (2025). Paternal SARS-CoV-2 infection impacts sperm small noncoding RNAs and increases anxiety in offspring in a sex-dependent manner. Nat. Commun. *16*, 9045. https://doi.org/10.1038/s41467-025-64473-0.

32. Morgan, C.P., Chan, J.C., and Bale, T.L. (2019). Driving the Next Generation: Paternal Lifetime Experiences Transmitted via Extracellular Vesicles and Their Small RNA Cargo. Biol. Psychiatry *85*, 164–171. https://doi.org/10.1016/j.biopsych.2018.09.007.

33. Xu, X., Miao, Z., Sun, M., and Wan, B. (2021). Epigenetic Mechanisms of Paternal Stress in Offspring Development and Diseases. International Journal of Genomics *2021*, 6632719. https://doi.org/10.1155/2021/6632719.

34. Liu, S., and Sharma, U. (2023). Sperm RNA Payload: Implications for Intergenerational Epigenetic Inheritance. Int. J. Mol. Sci. *24*, 5889. https://doi.org/10.3390/ijms24065889.

35. Chen, Q., Yan, W., and Duan, E. (2016). Epigenetic inheritance of acquired traits through sperm RNAs and sperm RNA modifications. Nat. Rev. Genet. *17*, 733–743. https://doi.org/10.1038/nrg.2016.106.

36. Machtinger, R., Laurent, L.C., and Baccarelli, A.A. (2016). Extracellular vesicles: roles in gamete maturation, fertilization and embryo implantation. Hum. Reprod. Update *22*, 182–193. https://doi.org/10.1093/humupd/dmv055.

37. Yuan, S., Schuster, A., Tang, C., Yu, T., Ortogero, N., Bao, J., Zheng, H., and Yan, W. (2016). Sperm-borne miRNAs and endo-siRNAs are important for fertilization and preimplantation embryonic development. Development *143*, 635–647. https://doi.org/10.1242/dev.131755.

38. Cui, L., Fang, L., Zhuang, L., Shi, B., Lin, C.-P., and Ye, Y. (2023). Sperm-borne microRNA-34c regulates maternal mRNA degradation and preimplantation embryonic development in mice. Reprod. Biol. Endocrinol. *21*, 40. https://doi.org/10.1186/s12958-023-01089-3.

39. Sun, Q., Li, Y., Yang, W., Feng, W., Zhou, J., Cao, Y., Zhang, B., Zhu, Z., and Han, C. (2024). CircMYH9/miR-133a-3p/CXCR4 axis: a novel regulatory network in sperm fertilization and embryo development. Molecular Biomedicine *5*, 69. https://doi.org/10.1186/s43556-024-00236-5.

40. Morgan, C.P., Shetty, A.C., Chan, J.C., Berger, D.S., Ament, S.A., Epperson, C.N., and Bale, T.L. (2020). Repeated sampling facilitates within- and between-subject modeling of the human sperm transcriptome to identify dynamic and stress-responsive sncRNAs. Sci. Rep. *10*, 17498. https://doi.org/10.1038/s41598-020-73867-7.

41. Zeid, D., and Gould, T.J. (2023). Chronic nicotine exposure alters sperm small RNA content in C57BL/6J mouse model. Dev. Psychobiol. *65*, e22367. https://doi.org/10.1002/dev.22367.

42. Gapp, K., Jawaid, A., Sarkies, P., Bohacek, J., Pelczar, P., Prados, J., Farinelli, L., Miska, E., and Mansuy, I.M. (2014). Implication of sperm RNAs in transgenerational inheritance of the effects of early trauma in mice. Nat. Neurosci. *17*, 667–669. https://doi.org/10.1038/nn.3695.

43. Roush, S., and Slack, F.J. (2008). The let-7 family of microRNAs. Trends Cell Biol. *18*, 505–516. https://doi.org/10.1016/j.tcb.2008.07.007.

44. Reinhart, B.J., Slack, F.J., Basson, M., Pasquinelli, A.E., Bettinger, J.C., Rougvie, A.E., Horvitz, H.R., and Ruvkun, G. (2000). The 21-nucleotide let-7 RNA regulates developmental timing in Caenorhabditis elegans. Nature *403*, 901–906. https://doi.org/10.1038/35002607.

45. Pasquinelli, A.E., Reinhart, B.J., Slack, F., Martindale, M.Q., Kuroda, M.I., Maller, B., Hayward, D.C., Ball, E.E., Degnan, B., Müller, P., et al. (2000). Conservation of the sequence and temporal expression of let-7 heterochronic regulatory RNA. Nature *408*, 86–89. https://doi.org/10.1038/35040556.

46. Han, L., Wang, Y., Wang, L., Guo, B., Pei, S., and Jia, Y. (2018). MicroRNA let-7f-5p regulates neuronal differentiation of rat bone marrow mesenchymal stem cells by targeting Par6α. Biochem. Biophys. Res. Commun. *495*, 1476–1481. https://doi.org/10.1016/j.bbrc.2017.11.024.

47. Liu, W., Chen, J., Yang, C., Lee, K.-F., Lee, Y.-L., Chiu, P.C.-N., zhang, Y., Duan, Y.-G., Liu, K., and Yeung, W.S.-B. (2022). Expression of microRNA let-7 in cleavage embryos modulates cell fate determination and formation of mouse blastocysts. Biol. Reprod. *107*, 1452–1463. https://doi.org/10.1093/biolre/ioac181.

48. Hamilton, M., Russell, S., Menezes, K., Moskovtsev, S.I., and Librach, C. (2022). Assessing spermatozoal small ribonucleic acids and their relationship to blastocyst development in idiopathic infertile males. Sci. Rep. *12*, 20010. https://doi.org/10.1038/s41598-022-24568-w.

49. Colas, A.R., McKeithan, W.L., Cunningham, T.J., Bushway, P.J., Garmire, L.X., Duester, G., Subramaniam, S., and Mercola, M. (2012). Whole-genome microRNA screening identifies let-7 and mir-18 as regulators of germ layer formation during early embryogenesis. Genes & Development *26*, 2567–2579. https://doi.org/10.1101/gad.200758.112.

50. Biondic, S., and Petropoulos, S. (2023). Evidence for Functional Roles of MicroRNAs in Lineage Specification During Mouse and Human Preimplantation Development. Yale J. Biol. Med. *96*, 481–494. https://doi.org/10.59249/fosi4358.

51. Barker, D.J.P., and Osmond, C. (1986). Infant mortality, childhood nutrition, and ischaemic heart disease in England and Wales. Lancet *327*, 1077–1081. https://doi.org/10.1016/S0140-6736(86)91340-1.

52. Barker, D.J., Eriksson, J.G., Forsén, T., and Osmond, C. (2002). Fetal origins of adult disease: strength of effects and biological basis. Int. J. Epidemiol. *31*, 1235–1239. https://doi.org/10.1093/ije/31.6.1235.

53. Barker, D.J.P. (2004). The Developmental Origins of Adult Disease. J. Am. Coll. Nutr. *23*, 588S–595S. https://doi.org/10.1080/07315724.2004.10719428.

54. Faa, G., Fanos, V., Manchia, M., Van Eyken, P., Suri, J.S., and Saba, L. (2024). The fascinating theory of fetal programming of adult diseases: A review of the fundamentals of the Barker hypothesis. Journal of Public Health Reasearch *13*, 22799036241226817. https://doi.org/10.1177/22799036241226817.

55. Proks, M., Salehin, N., and Brickman, J.M. (2025). Deep learning-based models for preimplantation mouse and human embryos based on single-cell RNA sequencing. Nat. Methods *22*, 207–216. https://doi.org/10.1038/s41592-024-02511-3.

56. Wang, X., Park, J., Susztak, K., Zhang, N.R., and Li, M. (2019). Bulk tissue cell type deconvolution with multi-subject single-cell expression reference. Nat. Commun. *10*, 380. https://doi.org/10.1038/s41467-018-08023-x.

57. Frum, T., and Ralston, A. (2015). Cell signaling and transcription factors regulating cell fate during formation of the mouse blastocyst. Trends Genet. *31*, 402–410. https://doi.org/10.1016/j.tig.2015.04.002.

58. Lacagnina, S. (2020). The Developmental Origins of Health and Disease (DOHaD). Am. J. Lifestyle Med. *14*, 47–50. https://doi.org/10.1177/1559827619879694.

59. Soubry, A. (2018). POHaD: why we should study future fathers. Environ. Epigenet. *4*, dvy007. https://doi.org/10.1093/eep/dvy007.

60. Lykke-Andersen, K., Gilchrist, M.J., Grabarek, J.B., Das, P., Miska, E., and Zernicka-Goetz, M. (2008). Maternal Argonaute 2 is essential for early mouse development at the maternal-zygotic transition. Mol. Biol. Cell *19*, 4383–4392. https://doi.org/10.1091/mbc.e08-02-0219.

61. Pauli, A., Rinn, J.L., and Schier, A.F. (2011). Non-coding RNAs as regulators of embryogenesis. Nat. Rev. Genet. *12*, 136–149. https://doi.org/10.1038/nrg2904.

62. Schulz, K.N., and Harrison, M.M. (2019). Mechanisms regulating zygotic genome activation. Nat. Rev. Genet. *20*, 221–234. https://doi.org/10.1038/s41576-018-0087-x.

63. Vastenhouw, N.L., Cao, W.X., and Lipshitz, H.D. (2019). The maternal-to-zygotic transition revisited. Development *146*, dev161471. https://doi.org/10.1242/dev.161471.

64. Rodgers, A.B., Morgan, C.P., Leu, N.A., and Bale, T.L. (2015). Transgenerational epigenetic programming via sperm microRNA recapitulates effects of paternal stress. Proc. Natl. Acad. Sci. *112*, 13699–13704. https://doi.org/10.1073/pnas.1508347112.

65. Marzi, M.J., Ghini, F., Cerruti, B., de Pretis, S., Bonetti, P., Giacomelli, C., Gorski, M.M., Kress, T., Pelizzola, M., Muller, H., et al. (2016). Degradation dynamics of microRNAs revealed by a novel pulse-chase approach. Genome Res. *26*, 554–565. https://doi.org/10.1101/gr.198788.115.

66. Jennings, G.T., Sechi, S., Stevenson, P.M., Tuckey, R.C., Parmelee, D., and McAlister-Henn, L. (1994). Cytosolic NADP(+)-dependent isocitrate dehydrogenase. Isolation of rat cDNA and study of tissue-specific and developmental expression of mRNA. J. Biol. Chem. *269*, 23128–23134. https://doi.org/10.1016/S0021-9258(17)31629-0.

67. Ochoa, S., Salles, J.B.V., and Ortiz, P.J. (1950). Biosynthesis of dicarboxylic acids by carbon dioxide fixation: III. Enzymatic synthesis of ι-malic acid by reductive carboxylation of pyruvic acid. J. Biol. Chem. *187*, 863–874. https://doi.org/10.1016/S0021-9258(18)56232-3.

68. Wermuth, B. (1981). Purification and properties of an NADPH-dependent carbonyl reductase from human brain. Relationship to prostaglandin 9-ketoreductase and xenobiotic ketone reductase. J. Biol. Chem. *256*, 1206–1213. https://doi.org/10.1016/S0021-9258(19)69950-3.

69. Nakanishi, M., Deyashiki, Y., Ohshima, K., and Hara, A. (1995). Cloning, Expression and Tissue Distribution of Mouse Tetrameric Carbonyl Reductase. Eur. J. Biochem. *228*, 381–387. https://doi.org/10.1111/j.1432-1033.1995.0381n.x.

70. Gardner, R.L. (1978). The Relationship Between Cell Lineage and Differentiation in the Early Mouse Embryo. In Genetic Mosaics and Cell Differentiation, W.J. Gehring, ed. (Springer Berlin Heidelberg), pp. 205–241. https://doi.org/10.1007/978-3-540-35803-9_8.

71. Niakan, K.K., Han, J., Pedersen, R.A., Simon, C., and Pera, R.A. (2012). Human pre-implantation embryo development. Development *139*, 829–841. https://doi.org/10.1242/dev.060426.

72. Leung, C.Y., and Zernicka-Goetz, M. (2015). Mapping the journey from totipotency to lineage specification in the mouse embryo. Curr. Opin. Genet. Dev. *34*, 71–76. https://doi.org/10.1016/j.gde.2015.08.002.

73. Lee, S.H., and Rinaudo, P.F. (2024). Metabolic regulation of preimplantation embryo development in vivo and in vitro: Molecular mechanisms and insights. Biochem. Biophys. Res. Commun. *726*, 150256. https://doi.org/10.1016/j.bbrc.2024.150256.

74. Darr, H., and Benvenisty, N. (2009). Genetic Analysis of the Role of the Reprogramming Gene LIN-28 in Human Embryonic Stem Cells. Stem Cell. *27*, 352–362. https://doi.org/10.1634/stemcells.2008-0720.

75. Sato, T., Okumura, F., Ariga, T., and Hatakeyama, S. (2012). TRIM6 interacts with Myc and maintains the pluripotency of mouse embryonic stem cells. J. Cell Sci. *125*, 1544–1555. https://doi.org/10.1242/jcs.095273.

76. Lim, L.S., Loh, Y.H., Zhang, W., Li, Y., Chen, X., Wang, Y., Bakre, M., Ng, H.H., and Stanton, L.W. (2007). Zic3 is required for maintenance of pluripotency in embryonic stem cells. Mol. Biol. Cell *18*, 1348–1358. https://doi.org/10.1091/mbc.e06-07-0624.

77. Jung, S., Ko, S.H., Ahn, N., Lee, J., Park, C.-H., and Hwang, J. (2024). Role of UPF1-LIN28A interaction during early differentiation of

pluripotent stem cells. Nat. Commun. *15*, 158. https://doi.org/10.1038/s41467-023-44600-5.

78. Lilly, A.J., Mazan, A., Scott, D.A., Lacaud, G., and Kouskoff, V. (2017). SOX7 expression is critically required in FLK1-expressing cells for vasculogenesis and angiogenesis during mouse embryonic development. Mech. Dev. *146*, 31–41. https://doi.org/10.1016/j.mod.2017.05.004.
79. Séguin, C.A., Draper, J.S., Nagy, A., and Rossant, J. (2008). Establishment of Endoderm Progenitors by SOX Transcription Factor Expression in Human Embryonic Stem Cells. Cell Stem Cell *3*, 182–195. https://doi.org/10.1016/j.stem.2008.06.018.
80. Boyerinas, B., Park, S.-M., Hau, A., Murmann, A.E., and Peter, M.E. (2010). The role of let-7 in cell differentiation and cancer. Endocr. Relat. Cancer *17*, F19–F36. https://doi.org/10.1677/erc-09-0184.
81. Schulman, B.R., Esquela-Kerscher, A., and Slack, F.J. (2005). Reciprocal expression of lin-41 and the microRNAs let-7 and mir-125 during mouse embryogenesis. Dev. Dyn. *234*, 1046–1054. https://doi.org/10.1002/dvdy.20599.
82. Fresa, K.J., Cheng, M.H., Larson, K.Y., Crook, A.A., Saviola, A.J., Gonzalez-Castro, R.A., Chen, T.W., and Carnevale, E.M. (2025). Delayed blastocyst development is associated with altered metabolism and proteome in male and female bovine embryos. Biol. Reprod. *112*, 1072–1085. https://doi.org/10.1093/biolre/ioaf058.
83. Sun, L., Wang, Y., Yang, M., Xu, Z.J., Miao, J., Bai, Y., and Lin, T. (2024). Delayed Blastocyst Formation Reduces the Quality and Hatching Ability of Porcine Parthenogenetic Blastocysts by Increasing DNA Damage, Decreasing Cell Proliferation, and Altering Transcription Factor Expression Patterns. J. Dev. Biol. *12*, 26. https://doi.org/10.3390/jdb12040026.
84. Morgan, C.P., and Bale, T.L. (2012). Sex differences in microRNA regulation of gene expression: no smoke, just miRs. Biol. Sex Differ. *3*, 22. https://doi.org/10.1186/2042-6410-3-22.
85. Patrat, C., Ouimette, J.-F., and Rougeulle, C. (2020). X chromosome inactivation in human development. Development *147*, dev183095. https://doi.org/10.1242/dev.183095.
86. Oikawa, M., Inoue, K., Shiura, H., Matoba, S., Kamimura, S., Hirose, M., Mekada, K., Yoshiki, A., Tanaka, S., Abe, K., et al. (2014). Understanding the X chromosome inactivation cycle in mice: a comprehensive view provided by nuclear transfer. Epigenetics *9*, 204–211. https://doi.org/10.4161/epi.26939.
87. Richardson, V., Engel, N., and Kulathinal, R.J. (2023). Comparative developmental genomics of sex-biased gene expression in early embryogenesis across mammals. Biol. Sex Differ. *14*, 30. https://doi.org/10.1186/s13293-023-00520-z.
88. Zhu, M., and Zernicka-Goetz, M. (2020). Living a Sweet Life: Glucose Instructs Cell Fate in the Mouse Embryo. Dev. Cell *53*, 1–2. https://doi.org/10.1016/j.devcel.2020.03.012.
89. Chi, F., Sharpley, M.S., Nagaraj, R., Roy, S.S., and Banerjee, U. (2020). Glycolysis-Independent Glucose Metabolism Distinguishes TE from ICM Fate during Mammalian Embryogenesis. Dev. Cell *53*, 9–26.e24. https://doi.org/10.1016/j.devcel.2020.02.015.
90. Kumar, R.P., Ray, S., Home, P., Saha, B., Bhattacharya, B., Wilkins, H.M., Chavan, H., Ganguly, A., Milano-Foster, J., Paul, A., et al. (2018). Regulation of energy metabolism during early mammalian development: TEAD4 controls mitochondrial transcription. Development *145*, dev162644. https://doi.org/10.1242/dev.162644.
91. Parenti, M., Schmidt, R.J., Tancredi, D.J., Hertz-Picciotto, I., Walker, C.K., and Slupsky, C.M. (2024). Neurodevelopment and Metabolism in the Maternal-Placental-Fetal Unit. JAMA Netw. Open *7*, e2413399. https://doi.org/10.1001/jamanetworkopen.2024.13399.
92. Oyarzábal, A., Musokhranova, U., Barros, L., and García-Cazorla, A. (2021). Energy metabolism in childhood neurodevelopmental disorders. EBioMedicine *69*, 103474. https://doi.org/10.1016/j.ebiom.2021.103474.
93. Parenti, M., and Slupsky, C.M. (2024). Disrupted Prenatal Metabolism May Explain the Etiology of Suboptimal Neurodevelopment: A Focus on Phthalates and Micronutrients and their Relationship to Autism Spectrum Disorder. Adv. Nutr. *15*, 100279. https://doi.org/10.1016/j.advnut.2024.100279.
94. He, Y., Xie, K., Yang, K., Wang, N., and Zhang, L. (2025). Unraveling the Interplay Between Metabolism and Neurodevelopment in Health and Disease. CNS Neurosci. Ther. *31*, e70427. https://doi.org/10.1111/cns.70427.
95. Lester, B.M., and Marsit, C.J. (2018). Epigenetic mechanisms in the placenta related to infant neurodevelopment. Epigenomics *10*, 321–333. https://doi.org/10.2217/epi-2016-0171.
96. Zeltser, L.M., and Leibel, R.L. (2011). Roles of the placenta in fetal brain development. Proc. Natl. Acad. Sci. USA *108*, 15667–15668. https://doi.org/10.1073/pnas.1112239108.
97. Kim, J.H., Lee, J.A., Song, Y.M., Park, C.H., Hwang, S.J., Kim, Y.S., Kaang, B.K., and Son, H. (2006). Overexpression of calbindin-D28K in hippocampal progenitor cells increases neuronal differentiation and neurite outgrowth. FASEB J. *20*, 109–111. https://doi.org/10.1096/fj.05-4826fje.
98. Bormuth, I., Yan, K., Yonemasu, T., Gummert, M., Zhang, M., Wichert, S., Grishina, O., Pieper, A., Zhang, W., Goebbels, S., et al. (2013). Neuronal Basic Helix–Loop–Helix Proteins Neurod2/6 Regulate Cortical Commissure Formation before Midline Interactions. J. Neurosci. *33*, 641–651. https://doi.org/10.1523/jneurosci.0899-12.2013.
99. Failli, V., Bachy, I., and Rétaux, S. (2002). Expression of the LIM-homeodomain gene Lmx1a (dreher) during development of the mouse nervous system. Mech. Dev. *118*, 225–228. https://doi.org/10.1016/S0925-4773(02)00254-X.
100. Lang, B., Zhang, L., Jiang, G., Hu, L., Lan, W., Zhao, L., Hunter, I., Pruski, M., Song, N.-N., Huang, Y., et al. (2016). Control of cortex development by ULK4, a rare risk gene for mental disorders including schizophrenia. Sci. Rep. *6*, 31126. https://doi.org/10.1038/srep31126.
101. Mattson, M.P., Rychlik, B., Chu, C., and Christakos, S. (1991). Evidence for calcium-reducing and excito-protective roles for the calcium-binding protein calbindin-D28k in cultured hippocampal neurons. Neuron *6*, 41–51. https://doi.org/10.1016/0896-6273(91)90120-o.
102. Liu, F., and Graybiel, A. (1992). Transient calbindin-D28k-positive systems in the telencephalon: ganglionic eminence, developing striatum and cerebral cortex. J. Neurosci. *12*, 674–690. https://doi.org/10.1523/jneurosci.12-02-00674.1992.
103. Stoner, R., Chow, M.L., Boyle, M.P., Sunkin, S.M., Mouton, P.R., Roy, S., Wynshaw-Boris, A., Colamarino, S.A., Lein, E.S., and Courchesne, E. (2014). Patches of disorganization in the neocortex of children with autism. N. Engl. J. Med. *370*, 1209–1219. https://doi.org/10.1056/NEJMoa1307491.
104. Whitney, E.R., Kemper, T.L., Bauman, M.L., Rosene, D.L., and Blatt, G.J. (2008). Cerebellar Purkinje cells are reduced in a subpopulation of autistic brains: a stereological experiment using calbindin-D28k. Cerebellum *7*, 406–416. https://doi.org/10.1007/s12311-008-0043-y.
105. Karlsson Linnér, R., Mallard, T.T., Barr, P.B., Sanchez-Roige, S., Madole, J.W., Driver, M.N., Poore, H.E., de Vlaming, R., Grotzinger, A.D., Tielbeek, J.J., et al. (2021). Multivariate analysis of 1.5 million people identifies genetic associations with traits related to self-regulation and addiction. Nat. Neurosci. *24*, 1367–1376. https://doi.org/10.1038/s41593-021-00908-3.
106. Bellido, T., Huening, M., Raval-Pandya, M., Manolagas, S.C., and Christakos, S. (2000). Calbindin-D28k is expressed in osteoblastic cells and suppresses their apoptosis by inhibiting caspase-3 activity. J. Biol. Chem. *275*, 26328–26332. https://doi.org/10.1074/jbc.M003600200.
107. Leal, C.R.V., Costa, L.B., Ferreira, G.C., Ferreira, A.d.M., Reis, F.M., and Simões e Silva, A.C. (2022). Renin-angiotensin system in normal pregnancy and in preeclampsia: A comprehensive review. Pregnancy Hypertens. *28*, 15–20. https://doi.org/10.1016/j.preghy.2022.01.011.

108. Meakin, A.S., Smith, M., Morrison, J.L., Roberts, C.T., Lappas, M., Ellery, S.J., Holland, O., Perkins, A., McCracken, S.A., Flenady, V., and Clifton, V.L. (2024). Placenta-Specific Transcripts Containing Androgen Response Elements Are Altered In Silico by Male Growth Outcomes. Int. J. Mol. Sci. *25*, 1688. https://doi.org/10.3390/ijms25031688.

109. Jang, H., Choi, Y., Yoo, I., Han, J., Kim, M., and Ka, H. (2017). Expression and regulation of prostaglandin transporters, ATP-binding cassette, subfamily C, member 1 and 9, and solute carrier organic anion transporter family, member 2A1 and 5A1 in the uterine endometrium during the estrous cycle and pregnancy in pigs. Asian-Australas. J. Anim. Sci. *30*, 643–652. https://doi.org/10.5713/ajas.16.0637.

110. Hayashi, K.G., Hosoe, M., Sakumoto, R., and Takahashi, T. (2013). Temporo-spatial expression of adrenomedullin and its receptors in the bovine placenta. Reprod. Biol. Endocrinol. *11*, 62. https://doi.org/10.1186/1477-7827-11-62.

111. Ge, L., Huang, P., Miao, H., Yu, H., Wu, D., Chen, F., Lin, Y., Lin, Y., Li, W., and Hua, J. (2023). The new landscape of differentially expression proteins in placenta tissues of gestational diabetes based on iTRAQ proteomics. Placenta *131*, 36–48. https://doi.org/10.1016/j.placenta.2022.11.012.

112. Genbacev, O., Donne, M., Kapidzic, M., Gormley, M., Lamb, J., Gilmore, J., Larocque, N., Goldfien, G., Zdravkovic, T., McMaster, M.T., and Fisher, S.J. (2011). Establishment of human trophoblast progenitor cell lines from the chorion. Stem Cell. *29*, 1427–1436. https://doi.org/10.1002/stem.686.

113. Kramer, A.C., Jansson, T., Bale, T.L., and Powell, T.L. (2023). Maternal-fetal cross-talk via the placenta: influence on offspring development and metabolism. Development *150*, dev202088. https://doi.org/10.1242/dev.202088.

114. Amar, A.P., and Weiss, M.H. (2003). Pituitary anatomy and physiology. Neurosurgery Clinics *14*, 11–23. https://doi.org/10.1016/S1042-3680(02)00017-7.

115. Duan, T., Du, Y., Xing, C., Wang, H.Y., and Wang, R.-F. (2022). Toll-Like Receptor Signaling and Its Role in Cell-Mediated Immunity. Front. Immunol. *ume*, 13–2022. https://doi.org/10.3389/fimmu.2022.812774.

116. Glennon, E., Kaunzner, U.W., Gagnidze, K., McEwen, B.S., and Bulloch, K. (2015). Pituitary dendritic cells communicate immune pathogenic signals. Brain Behav. Immun. *50*, 232–240. https://doi.org/10.1016/j.bbi.2015.07.007.

117. Hoek, A., Allaerts, W., Leenen, P., Schoemaker, J., and Drexhage, H. (1997). Dendritic cells and macrophages in the pituitary and the gonads. Evidence for their role in the fine regulation of the reproductive endocrine response. Eur. J. Endocrinol. *136*, 8–24. https://doi.org/10.1530/eje.0.1360008.

118. Verma, A., Huffman, J.E., Rodriguez, A., Conery, M., Liu, M., Ho, Y.L., Kim, Y., Heise, D.A., Guare, L., Panickan, V.A., et al. (2024). Diversity and scale: Genetic architecture of 2068 traits in the VA Million Veteran Program. Science *385*, eadj1182. https://doi.org/10.1126/science.adj1182.

119. He, D., Liu, H., Wei, W., Zhao, Y., Cai, Q., Shi, S., Chu, X., Qin, X., Zhang, N., Xu, P., and Zhang, F. (2023). A longitudinal genome-wide association study of bone mineral density mean and variability in the UK Biobank. Osteoporos. Int. *34*, 1907–1916. https://doi.org/10.1007/s00198-023-06852-1.

120. Loya, H., Kalantzis, G., Cooper, F., and Palamara, P.F. (2025). A scalable variational inference approach for increased mixed-model association power. Nat. Genet. *57*, 461–468. https://doi.org/10.1038/s41588-024-02044-7.

121. Yengo, L., Vedantam, S., Marouli, E., Sidorenko, J., Bartell, E., Sakaue, S., Graff, M., Eliasen, A.U., Jiang, Y., Raghavan, S., et al. (2022). A saturated map of common genetic variants associated with human height. Nature *610*, 704–712. https://doi.org/10.1038/s41586-022-05275-y.

122. Shi, S., Rubinacci, S., Hu, S., Moutsianas, L., Stuckey, A., Need, A.C., Palamara, P.F., Caulfield, M., Marchini, J., and Myers, S. (2024). A Genomics England haplotype reference panel and imputation of UK Biobank. Nat. Genet. *56*, 1800–1803. https://doi.org/10.1038/s41588-024-01868-7.

123. Pietzner, M., Wheeler, E., Carrasco-Zanini, J., Cortes, A., Koprulu, M., Wörheide, M.A., Oerton, E., Cook, J., Stewart, I.D., Kerrison, N.D., et al. (2021). Mapping the proteo-genomic convergence of human diseases. Science *374*, eabj1541. https://doi.org/10.1126/science.abj1541.

124. Schoeler, T., Pingault, J.B., and Kutalik, Z. (2025). Combining cross-sectional and longitudinal genomic approaches to identify determinants of cognitive and physical decline. Nat. Commun. *16*, 4524. https://doi.org/10.1038/s41467-025-59383-0.

125. Morrison, K.E., Jašarević, E., Howard, C.D., and Bale, T.L. (2020). It's the fiber, not the fat: significant effects of dietary challenge on the gut microbiome. Microbiome *8*, 15. https://doi.org/10.1186/s40168-020-0791-6.

126. Mínguez-Alarcón, L., Williams, P.L., Souter, I., Ford, J.B., Hauser, R., and Chavarro, J.E. (2024). Women's preconception psychological stress and birth outcomes in a fertility clinic: the EARTH study. Front Glob Womens Health *5*, 1293255. https://doi.org/10.3389/fgwh.2024.1293255.

127. An, Y., Sun, Z., Li, L., Zhang, Y., and Ji, H. (2013). Relationship between psychological stress and reproductive outcome in women undergoing in vitro fertilization treatment: psychological and neurohormonal assessment. J. Assist. Reprod. Genet. *30*, 35–41. https://doi.org/10.1007/s10815-012-9904-x.

128. Nakamura, K., Sheps, S., and Arck, P.C. (2008). Stress and reproductive failure: past notions, present insights and future directions. J. Assist. Reprod. Genet. *25*, 47–62. https://doi.org/10.1007/s10815-008-9206-5.

129. Seok, H., Lee, H., Jang, E.S., and Chi, S.W. (2018). Evaluation and control of miRNA-like off-target repression for RNA interference. Cell. Mol. Life Sci. *75*, 797–814. https://doi.org/10.1007/s00018-017-2656-0.

130. Love, M.I., Huber, W., and Anders, S. (2014). Moderated estimation of fold change and dispersion for RNA-seq data with DESeq2. Genome Biol. *15*, 550. https://doi.org/10.1186/s13059-014-0550-8.

131. Chen, Y., and Wang, X. (2020). miRDB: an online database for prediction of functional microRNA targets. Nucleic Acids Res. *48*, D127–D131. https://doi.org/10.1093/nar/gkz757.

132. Sticht, C., De La Torre, C., Parveen, A., and Gretz, N. (2018). miRWalk: An online resource for prediction of microRNA binding sites. PLoS One *13*, e0206239. https://doi.org/10.1371/journal.pone.0206239.

133. Lewis, B.P., Burge, C.B., and Bartel, D.P. (2005). Conserved Seed Pairing, Often Flanked by Adenosines, Indicates that Thousands of Human Genes are MicroRNA Targets. Cell *120*, 15–20. https://doi.org/10.1016/j.cell.2004.12.035.

134. McGeary, S.E., Lin, K.S., Shi, C.Y., Pham, T.M., Bisaria, N., Kelley, G.M., and Bartel, D.P. (2019). The biochemical basis of microRNA targeting efficacy. Science *366*, eaav1741. https://doi.org/10.1126/science.aav1741.

135. Kassambara, A., and Mundt, F. (2020). factoextra: Extract and Visualize the Results of Multivariate Data Analyses. R package version 1.0.7. https://github.com/kassambara/factoextra.

136. Kolberg, L., Raudvere, U., Kuzmin, I., Vilo, J., and Peterson, H. (2020). gprofiler2 – an R package for gene list functional enrichment analysis and namespace conversion toolset g:Profiler. F1000Res. *9*, ELIXIR-709. https://doi.org/10.12688/f1000research.24956.2.

137. Szklarczyk, D., Kirsch, R., Koutrouli, M., Nastou, K., Mehryary, F., Hachilif, R., Gable, A.L., Fang, T., Doncheva, N.T., Pyysalo, S., et al. (2023). The STRING database in 2023: protein-protein association networks and functional enrichment analyses for any sequenced genome of interest. Nucleic Acids Res. *51*, D638–D646. https://doi.org/10.1093/nar/gkac1000.

138. Xu, S., Hu, E., Cai, Y., Xie, Z., Luo, X., Zhan, L., Tang, W., Wang, Q., Liu, B., Wang, R., et al. (2024). Using clusterProfiler to characterize multiomics data. Nat. Protoc. *19*, 3292–3320. https://doi.org/10.1038/s41596-024-01020-z.

139. Christensen, R. (2025). _ordinal-Regression Models for Ordinal Data_. R package version 12-4.1. https://CRAN.R-project.org/package=ordinal.

140. Lüdecke, D. (2018). ggeffects: Tidy data frames of marginal effects from regression models. J. Open Source Softw. *3*, 772. https://doi.org/10.21105/joss.00772.

141. Kiani, J., and Rassoulzadegan, M. (2013). A load of small RNAs in the sperm — how many bits of hereditary information? Cell Res. *23*, 18–19. https://doi.org/10.1038/cr.2012.181.

142. Kawano, M., Kawaji, H., Grandjean, V., Kiani, J., and Rassoulzadegan, M. (2012). Novel small noncoding RNAs in mouse spermatozoa, zygotes and early embryos. PLoS One *7*, e44542. https://doi.org/10.1371/journal.pone.0044542.

143. Mehta, P., and Singh, R. (2025). The composition of human sperm sncRNAome: a cross-country small RNA profiling. Reprod. Biol. Endocrinol. *23*, 36. https://doi.org/10.1186/s12958-025-01358-3.

144. Jašarević, E., Hill, E.M., Kane, P.J., Rutt, L., Gyles, T., Folts, L., Rock, K.D., Howard, C.D., Morrison, K.E., Ravel, J., and Bale, T.L. (2021). The composition of human vaginal microbiota transferred at birth affects offspring health in a mouse model. Nat. Commun. *12*, 6289. https://doi.org/10.1038/s41467-021-26634-9.

145. Bolger, A.M., Lohse, M., and Usadel, B. (2014). Trimmomatic: a flexible trimmer for Illumina sequence data. Bioinformatics *30*, 2114–2120. https://doi.org/10.1093/bioinformatics/btu170.

146. Bray, N.L., Pimentel, H., Melsted, P., and Pachter, L. (2016). Near-optimal probabilistic RNA-seq quantification. Nat. Biotechnol. *34*, 525–527. https://doi.org/10.1038/nbt.3519.

147. Ewels, P., Magnusson, M., Lundin, S., and Käller, M. (2016). MultiQC: summarize analysis results for multiple tools and samples in a single report. Bioinformatics *32*, 3047–3048. https://doi.org/10.1093/bioinformatics/btw354.

148. Ignatiadis, N., Klaus, B., Zaugg, J.B., and Huber, W. (2016). Data-driven hypothesis weighting increases detection power in genome-scale multiple testing. Nat. Methods *13*, 577–580. https://doi.org/10.1038/nmeth.3885.

149. Zhu, A., Ibrahim, J.G., and Love, M.I. (2019). Heavy-tailed prior distributions for sequence count data: removing the noise and preserving large differences. Bioinformatics *35*, 2084–2092. https://doi.org/10.1093/bioinformatics/bty895.

STAR★METHODS

KEY RESOURCES TABLE

REAGENT or RESOURCE	SOURCE	IDENTIFIER
Chemicals, peptides, and recombinant proteins		
Pregnant mare's serum gonadotropin (PMSG)	Medix Biochemica	Cat#493-10
Human chorionic gonadotropin (hCG)	Sigma-Aldrich	Cat#CG5-1VL
Trizol reagent	ThermoFisher	Cat#15596026
Critical commercial assays		
PicoPure™ RNA Isolation Kit	Applied Biosystems	Cat#KIT0204
SMARTer® Stranded Total RNA-Seq Kit v3 - Pico Input Mammalian	Takara Bio	Cat#634486
TruSeq Stranded mRNA Library Prep	Illumina	Cat#20020595
TruSeq Stranded Total RNA Library Prep	Illumina	Cat#20020596
^{125}I-corticosterone radioimmunoassay	MP Biomedicals	Cat#0712010-CF
Deposited data		
Blastocyst bulk RNA sequencing (raw data)	This paper	GEO: GSE314398
Fetal bulk RNA sequencing (raw data)	This paper	GEO: GSE314467
Placental bulk RNA sequencing (raw data)	This paper	GEO: GSE314710
Pituitary bulk RNA sequencing (raw data)	This paper	GEO: GSE314713
Single-cell preimplantation embryo RNA sequencing reference dataset (raw data)	Proks et al.[55]	https://huggingface.co/spaces/brickmanlab/hf-preimplantation-portal
Experimental models: Organisms/strains		
C57BL/6J females	Jackson Laboratories	Strain#000664; RRID: IMSR_JAX:000664
129S1/SvImJ males	Jackson Laboratories	Strain#002448; RRID: IMSR_JAX:002448
Hsd:ICR (CD-1) vasectomized males	Envigo	Order#030; RRID: IMSR_ENV:HSD-030
Hsd:ICR (CD-1) females	Envigo	Order#030; RRID: IMSR_ENV:HSD-030
Oligonucleotides		
Let-7f-5p miRCURY LNA miRNA Mimic: UGAGGUAGUAGAUUGUAUAGUU	Qiagen	Cat#YM00471944
Software and algorithms		
R (version 4.5.1)	https://www.r-project.org/	RRID: SCR_001905; https://www.r-project.org/
DESeq2 (version 1.48.2)	Love et al.[130]	RRID: SCR_015687; https://bioconductor.org/packages/release/bioc/html/DESeq2.html
miRDB (version 6.0)	Chen et al.[131]	RRID: SCR_010848; http://mirdb.org/miRDB/
miRWalk (version 3.0)	Sticht et al.[132]	RRID: SCR_016509; http://mirwalk.umm.uni-heidelberg.de/
TargetScan (version 8.0)	Lewis et al.[133]; McGeary et al.[134]	RRID: SCR_010845; http://targetscan.org/
factoextra (version 1.0.7)	Kassambara et al.[135]	RRID: SCR_016692; https://cran.r-project.org/web/packages/factoextra/index.html
gprofiler2 (version 0.2.3)	Kolberg et al.[136]	RRID: SCR_018190; https://cran.r-project.org/web/packages/gprofiler2/index.html
Multi-subject Single Cell Deconvolution (MuSiC; version 1.0.0)	Wang et al.[56]	https://xuranw.github.io/MuSiC/articles/MuSiC.html
STRINGdb (version 2.20.0)	Szklarczyk et al.[137]	https://string-db.org/
clusterProfiler (version 4.16.0)	Xu et al.[138]	RRID: SCR_016884; https://bioconductor.org/packages/release/bioc/html/clusterProfiler.html
ordinal (version 12-4.1)	Christensen[139]	RRID: SCR_022856; https://cran.r-project.org/package=ordinal
ggeffects (version 2.3.1)	Lüdecke[140]	RRID: SCR_022496; https://cran.r-project.org/package=ggeffects
GraphPad Prism (version 10.5.0)	http://www.graphpad.com/	RRID: SCR_002798; http://www.graphpad.com/

EXPERIMENTAL MODEL AND STUDY PARTICIPANT DETAILS

Study approval

All studies were performed according to experimental protocols approved by the University of Colorado Institutional Animal Care and Use Committee (#01216), and all procedures were conducted in accordance with the NIH Guide for the Care and Use of Laboratory Animals. Male 129S1/SvImJ and female C57BL/6 J mice were obtained from Jackson Laboratories to produce C57BL/6:129 F1 hybrid embryos. Hsd:ICR (CD-1) vasectomized males and Hsd:ICR (CD-1) females were obtained from Envigo for embryo transfer studies.

All mice were housed in a 14:10 light:dark cycle (6:00 lights on, 19:00 lights off) with temperature 22 C and relative humidity 37%. Food (Teklad 2920X irradiated rodent diet) and water were provided *ad libitum*. All animals were group housed prior to breeding. Following breeding and embryo transfers, males and pregnant females were singly housed.

Embryo microinjections

4-8 week old C57BL/6 J females were super-ovulated via intraperitoneal injection of 5 IU of pregnant mare's serum gonadotropin (PMSG) (Medix Biochemica, 493-10) followed by 5 IU of human chorionic gonadotropin (hCG) (Sigma-Aldrich, CG5-1VL) 48 h later. Females were then paired with 8 week old 129S1/SvImJ sires. Breeding pairs were separated the next morning following confirmation of a copulatory plug. Fertilized F1 hybrid embryos were dissected from the ampulla of the oviduct 14–16 h after hCG administration. To remove the cumulus cells, embryos were incubated in CZB-HEPES media (Sigma-Aldrich, MR-019) supplemented with 3 mg/mL hyaluronidase (Sigma-Aldrich, H4272) for 2–3 min at room temperature.

Zygotes were randomly assigned for microinjection of nuclease-free water (vehicle) or a let-7f-5p mimic as previously described.[64] The let-7f miRCURY LNA microRNA (miRNA) Mimic (Qiagen, YM00471944, UGAGGUAGUAGAUUGUAUAGUU) was resuspended in the same nuclease-free water used for vehicle injections. We previously calculated the quantity of mimic sufficient to emulate biologically relevant elevated levels of miRNA delivered via mature mammalian sperm cells to be ~0.01 fg.[64,141–143] Accordingly, the stress-relevant injection concentration (let-7f) was 5 μM, with a target of reaching ~0.01 fg of let-7f mimic delivery. This second concentration (2× let-7f) was selected to emulate supraphysiological levels as validation of the specificity of the miRNA mimic.

Embryo culture and transfer

Injected zygotes were cultured in potassium-supplemented simplex optimized medium (KSOM, Sigma-Aldrich, MR-121) at 37 C in a humidified atmosphere of 5% CO_2 and 5% O_2. The KSOM culture drops were covered with light mineral oil (Sigma-Aldrich, ES-005) to prevent evaporation. For embryo transfers, CD-1 females were synchronized by mating with vasectomized males and those with a copulatory plug were selected as recipients. Embryos were surgically transferred into the oviducts of recipient dams.

For blastocyst RNA sequencing, embryos were cultured until the appropriate stage and then were pooled and flash frozen in liquid nitrogen. They were stored at −80 C until RNA isolation. A total of $N = 80$ vehicle ($N = 8$ pooled), $N = 110$ let-7f ($N = 11$ pooled), and $N = 50$ 2× let-7f ($N = 5$ pooled) blastocysts were retrieved. RNA isolation and sequencing were successful for $N = 7$ pooled vehicle samples, $N = 8$ pooled let-7f samples, and $N = 5$ pooled 2× let-7f samples.

For fetal and placental RNA sequencing, embryos were cultured until the blastocyst stage to ensure only successfully developing embryos were transferred. Blastocysts ($N = 7$ per group) from both groups were surgically transferred into the same 8 week old pseudo-pregnant CD-1 recipient dams ($N = 9$) to control for *in utero* environment, with right and left oviduct placement randomized.

At gestational day 12.5 (E12.5), pregnant females were euthanized, and fetoplacental units were harvested. The number of implantation sites was recorded and compared with the number of transferred embryos. Fetuses were dissected from the decidua and examined for viability. Fetuses exhibiting normal morphology and a visible heartbeat were classified as viable, whereas those with abnormal morphology and no detectable heartbeat were classified as non-viable. Viable fetuses and placentas were flash frozen in liquid nitrogen and stored at −80 C. A total of $N = 19$ vehicle and $N = 11$ let-7f fetoplacental units were harvested. Fetal RNA isolation and sequencing was successful for $N = 9$ vehicle (5 females, 4 males) and $N = 5$ let-7f (3 females, 2 males). Placental RNA isolation and sequencing was successful for $N = 9$ vehicle (4 females, 5 males) and $N = 9$ let-7f (6 females, 3 males).

For offspring studies, given that let-7f embryos did successfully implant, embryos ($N = 10$–15) were surgically transferred into the oviduct of 8 week old pseudo-pregnant CD-1 recipient dams ($N = 6$ per group) at the 2-cell stage to minimize culture time. Only litters with at least $N = 4$ pups were included in our studies.

METHOD DETAILS

RNA isolation and library prep of blastocysts

Embryos were pooled into samples of $N = 10$ to provide adequate material to isolate high-quality RNA. Total RNA was extracted from frozen embryos using the PicoPure RNA Isolation Kit (Applied Biosystems, KIT0204) according to manufacturer's instructions for isolation from cell pellets with DNase treatment. RNA quality and concentration were confirmed with the Bioanalyzer RNA 6000 Pico (Agilent, 5067-1513). Libraries of embryo rRNA-depleted total RNA were prepared with the SMARTer Stranded Total RNA-Seq Kit v3 - Pico Input Mammalian (Takara Bio, 634486) using 632 pg of total RNA. The High Sensitivity D1000 ScreenTape assay (Agilent, 5067–5584/5) and the Qubit 1× dsDNA High Sensitivity assay (ThermoFisher, Q33231) was used to verify quality and to quantify cDNA libraries. Samples were multiplexed into a single pool and sequenced using an Illumina NovaSEQ X.

RNA isolation and library prep of E12.5 tissues

Fetal and placental tissues were homogenized in 1 mL of Trizol reagent (ThermoFisher, 15596026) using the RNA-02 program on the gentleMACS Dissociator (Miltenyi Biotec, 130-093-235). Samples were centrifuged at 2000 x g for 1 min at 4 C, and the supernatant was transferred to a new nuclease-free tube. 0.2 mL of chloroform was added to each sample, and then samples were shaken vigorously for 15 s. Following 2–3 min incubation at room temperature, samples were centrifuged at 12,000 x g for 15 min at 4 C. RNA isolation proceeded with the aqueous phase using the RNeasy Kit (Qiagen, 75144) with DNase treatment. RNA quality was confirmed with the RNA ScreenTape Assay (Agilent, 5067–5576/77/78) and quantification was conducted using the Qubit RNA Broad Range Assay Kit (ThermoFisher, Q10210/11). Libraries of fetal and placental Poly-A selected mRNA were prepared with the TruSeq Stranded mRNA Library Prep (Illumina, 20020595) using 1 μg of total RNA. The High Sensitivity D1000 ScreenTape assay (Agilent, 5067–5584/5) and the Qubit 1× dsDNA High Sensitivity assay (ThermoFisher, Q33231) was used to verify quality and quantify cDNA libraries. Samples were multiplexed into a single pool and sequenced using an Illumina NovaSEQ X.

RNA isolation and library prep of adult pituitary glands

Pituitary glands were harvested and frozen in liquid nitrogen from 7 week old offspring. Samples were stored at −80 C until further processing.

Samples were homogenized in 500 μL of Trizol reagent (ThermoFisher, 15596026) using the RNA-02 program on the gentleMACS Dissociator (Miltenyi Biotec, 130-093-235). Samples were centrifuged at 3000 x g for 2 min at 4 C, and the supernatant was transferred to a new nuclease-free tube. 0.1 mL of chloroform was added to each sample, and then samples were shaken vigorously for 15 s. Following 2–3 min incubation at room temperature, samples were centrifuged at 12,000 x g for 15 min at 4 C. RNA isolation proceeded with the aqueous phase using the RNeasy Kit (Qiagen, 74104) with DNase treatment. RNA quality was confirmed with the RNA ScreenTape Assay (Agilent, 5067–5576/77/78) and quantification was conducted using the Qubit RNA Broad Range Assay Kit (ThermoFisher, Q10210/11). Libraries of rRNA-depleted total RNA were prepared with the TruSeq Stranded Total RNA Library Prep (Illumina, 20020596) using 0.221 μg of total RNA. The High Sensitivity D1000 ScreenTape assay (Agilent, 5067–5584/5) and the Qubit 1× dsDNA High Sensitivity assay (ThermoFisher, Q33231) was used to verify quality and quantify cDNA libraries. Samples were multiplexed into a single pool and sequenced using an Illumina NovaSEQ X.

Time-lapse imaging of preimplantation embryos

Following microinjections, each embryo was placed into a well of a 384-well plate (Corning, 3680) filled with 50 μL of KSOM culture medium and 50 μL of light mineral oil. A total of $N = 20$ embryos were plated for each group. The 384-well plate was placed inside of a MICA Microhub system (Leica, 11889182) with incubator settings of 5% CO_2, 37 C, and 63% humidity. Time-lapse imaging began around 15:00 on the day of harvest and continued for 96 h, with images taken every hr. Developmental stage was recorded as an ordered categorical variable with six levels: zygote, 2-cell, 4-cell, 8-cell, morula, and blastocyst. Each embryo contributed repeated observations across time and was staged by two blinded individuals (coders). As soon as an embryo began to transition, they were marked as the next stage. The two ratings were averaged to give the final stages as plotted.

Hypothalamus-pituitary-adrenal (HPA) axis assessment

HPA axis reactivity to a 15 min restraint was tested in 8 week old offspring animals as previously described.[29] 10 μL of tail blood was collected from mice at 0, 15, 30, and 120 min, immediately mixed with 50 mM EDTA, and kept on ice until the end of the assay. Blood samples were centrifuged for 10 min at 1500 x g. 3.02 μL of plasma was collected and stored at −80 C until analysis. Corticosterone levels were determined by ^{125}I-corticosterone radioimmunoassay (MP Biomedicals, 0712010-CF) following kit instructions.

24-h food consumption

To determine food consumption in 9 week old offspring animals, individually housed mice were given pre-weighed pellets of standard chow in new cages at 15:00. Pellets were weighed again the following day at the same time. Weight of food consumed was normalized to body weight of mice at the time of the assay.

Glucose tolerance test

Glucose tolerance of 11 week old offspring animals was measured as previously described.[144] Food was removed at 07:00 and mice were fasted for 2 h. Baseline glucose readings were collected by tail blood using the Contour Next Blood Glucose Monitoring System (Bayer Co, Germany). Mice were then injected intraperitoneally with 0.3 g/mL glucose in saline. Subsequent glucose readings were collected at 15, 30, 60, 90, 120 min.

QUANTIFICATION AND STATISTICAL ANALYSIS

RNA sequencing analyses

RNA sequencing data was trimmed using *Trimmomatic* (version 0.39) and aligned with reference genome GRCm39 from Ensembl using *kallisto* (version 0.50.1).[145,146] Quality was confirmed with *fastqc* (version 0.12.1) and *multiqc* (version 1.28).[147] Differential gene expression analysis was conducted in R (version 4.5.1) using *DESeq2* (version 1.48.2).[130] Log fold change shrinkage and

independent hypothesis weighting were utilized in the analyses.[148,149] Unidentified genes were excluded from visualizations. Predicted targets of let-7f included genes that were identified by at least 2 out of the 3 following miRNA target prediction databases: *miRDB* (version 6.0), *miRWalk* (version 3.0), and *TargetScan* (version 8.0).[131–134]

To determine sex enrichment of pooled blastocyst samples, normalized gene expression values (derived using the "median of ratios" method) of all genes located on the Y chromosome were averaged separately for each sample. These values were used as input features for unsupervised k-means clustering. The optimal number of clusters was determined using the elbow method, and clustering was performed with $k = 2$ to separate samples based on sex-associated expression patterns using *factoextra* (version 1.0.7).[135]

Gene ontology (GO) functional enrichment analysis was performed using *gprofiler2* (version 0.2.3).[136] Cell type deconvolution of blastocyst RNA sequencing was performed using a reference single-cell RNA sequencing dataset from Proks et al. and *Multi-subject Single Cell Deconvolution* (*MuSiC*, version 1.0.0).[55,56] Differences in cell type percentages were analyzed using Wilcoxon Rank-Sum Tests with FDR correction for multiple comparisons. Protein-protein interaction (PPI) network analyses utilized *STRINGdb* (version 2.20.0; https://string-db.org/) with a minimum interaction score of 0.700.[137] Gene Set Enrichment Analysis (GSEA) was performed using our gene sets ranked by Log_2 Fold Change (LFC) and *clusterProfiler* (version 4.16.0).[138]

RNA sequencing of blastocysts, fetuses, and placentas employed LFC threshold $\geq |1|$ and adjusted p cutoff ≤ 0.05. RNA sequencing of pituitary glands utilized LFC threshold $\geq |0.1|$ and adjusted p cutoff ≤ 0.05. As transcriptomic differences in the pituitary were analyzed months after the initial microinjection at the zygote stage, we hypothesized we would find subtle differences and utilized LFC threshold $\geq |0.1|$ to capture those. Benjamini-Hochberg procedure was used to correct for multiple comparisons. For GO functional enrichment analysis and PPI functional enrichment analysis, terms with FDR <0.05 were reported. For GSEA, gene sets with adjusted $p < 0.05$ (adjusted with Benjamini-Hochberg procedure).

Time-lapse imaging analysis

To model developmental progression of preimplantation embryos, a cumulative link mixed model was employed using *ordinal* (version 12-4.1) in R.[139] The outcome variable was embryo stage, and time in hr was modeled flexibly with natural cubic splines (5 degrees of freedom) to capture nonlinear developmental trajectories. Fixed effects included the interaction of time and treatment group, and coder identity, to adjust for inter-coder variation. A random intercept for embryo ID was included to account for repeated measures within embryos. The model was fit with a logit link and estimated via the Laplace approximation:

$$\text{stage}_{ij} \sim \text{ns}(\text{time}_{ij}, df = 5) * \text{group}_i + \text{coder}_i + (1|\text{embryo ID}_i)$$

where i indexes embryos and j indexes time points.

Model coefficients were reported as log-odds and exponentiated odds ratios (ORs) with 95% confidence intervals. Group differences were visualized through predicted probabilities of being in each developmental stage over time, generated with *ggeffects* (version 2.3.1).[140]

Additional analyses

The following statistical analyses were performed using GraphPad Prism (version 10.5.0). Percent of embryo development and fetal viability were analyzed by Chi-Square tests. For embryo development, post-hoc pairwise Chi-Square tests with Bonferroni correction were conducted. Percent of successful embryo transfers and sex ratios were also analyzed with Chi-Square tests. Weekly body weight measurements, corticosterone levels, and glucose levels were analyzed by two-way ANOVA with time as a repeated measure. When ANOVA assumptions were not met, a linear-mixed effects model was employed in R Studio using *lme4* (version 1.1–38). Body weight at 8 weeks, total weight gained, long bone length, litter size, gestational age at birth (GAB), and food consumed (in grams and normalized) were analyzed by unpaired two-tailed Student's t-tests. Significance was set at $p \leq 0.05$. All analyses are summarized in Table S10. Investigators were blinded to treatment groups for all experiments and analyses. Statistical details for all experiments are reported in the Results section and figure legends.